Quantification of Error Sources with Inertia Measurement Units in Sports

by

Haye Kamstra

In partial fulfillment to obtain the degree of Master of Science
at the Delft University of Technology

Master Mechancial Engineering
Track BioMechanical Design
Specialisation BioInspired Technology

Student number: 4469526
Supervisors: Prof. Dr. F.C.T. van der Helm, TU Delft
Msc. E. Wilmes, VU Amsterdam, KNVB

A thesis presented and defended on 01-11-2022

Department of Biomechanical Engineering
Faculty of Machanical, Maritime and Materials Engineering
Delft University of Technology
The Netherlands

Preface

During the last decades, both the size and production costs of sensors like Inertial Measurement Units (IMUs) has considerably decreased. This has opened the door for a wide variety of new applications, among which human motion analysis. Human motion analysis is applied in medical diagnosis, rehabilitation and performance registration in sports. IMUs have the great benefit over other human motion capture techniques that can be used outside a laboratory environment and therefore have large potential for numerous human motion analysis applications. The research project Citius, Altius, Sanius aims to realize this potential. In a collaboration between several universities and the Dutch Football Association the Smart Sensor Shorts are developed. The Smart Sensor Shorts are compression shorts with integrated IMUs that can be used to capture the load on the lower body in a much more specific way than other methods. However, there are still some challenges in this project. One of these are the errors present in the IMU measurements. Studies have validated IMUs and described their different sources of error. However, these errors have never been quantified during high intensity, dynamic movements. Furthermore have these errors never been separately quantified for the different sources of error. The study described in this thesis aims to fill this gap in literature. By defining and constructing local body frames in various ways, a method was developed to quantify each of the sources of error separately. These errors were quantified for different calibration techniques, movements and movement intensities. The results showed that the error of the definition of the body frames was the largest contributor to the total error and that the body segment, type of movement and movement intensity all had significant effect on the different sources of error. These findings provide additional insight for the use of IMUs in sport applications. Furthermore allows the developed method for the optimization of error reduction techniques.

To allow other sport scientists to benefit from the developed method, the data and data processing scripts were structured and open source shared. This enables other researchers to investigate what the influence of IMU calibration techniques, raw data filters and orientation filters have on the errors and allows them to optimize for the specific body segment, type of movement and movement intensity.

Furthermore was this thesis also converted into an article, currently under review for the journal Sensors. This thesis was produced solely by Haye Kamstra, with feed back from Erik Wilmes and Frans van der Helm and the produced article was co-authored by all three. The article is included in the second appendix of this thesis.

The author would like to thankfully acknowledge the Dutch Royal Football Association (KNVB) for the access to their research facility, Prof. Dr. Frans van der Helm for his constructive feedback that helped shape this thesis and especially MSc Erik Wilmes for all his advice and the very pleasant collaboration.

Haye Kamstra, October 2022

Quantification of Error Sources with Inertia Measurement Units in Sports

Kamstra, H. (4469526)
Master Thesis, TU Delft, Master Mechanical Engineering, Track Bio-Mechanical Design
Supervisors: Prof. Dr. F. Van der Helm, MSc E. Wilmes

Abstract— **Inertial measurement units (IMUs) offer the possibility to capture the lower body kinematics of players of outdoor team sports. However, various sources of error are present when using IMUs: the definition of the body frames, the soft tissue artefact (STA) and the orientation filter. Methods to minimize these errors are currently being used without knowing their exact influence on the various sources of errors. The goal of this study was to quantify each of the sources of error of an IMU. An optoelectronic system was used as a golden standard. Rigid marker clusters (RMCs) were designed to construct a rigid connection between the IMU and four markers. This allowed for the separate quantification of each of the sources of error. Ten subjects performed nine different trials, varying both in type of movement and in movement intensity. The error of the definition of the body frames (11.3-18.7 deg RMSD), the STA (3.8-9.1 deg RMSD) and the error of the orientation filter (3.0-12.7 deg RMSD) were all quantified separately. Furthermore, the type of movement, movement intensity and body segment were found to have a significant influence on the errors. This study is the first study to quantify each of these sources separately and allows future studies to quantify and optimize error reduction techniques.**

I. Introduction

A. Human Motion Analysis

Human motion analysis can be used for medical diagnosis, rehabilitation and improved performance in sports[1]. Currently the most used method for human motion analysis is stereophotogrammetry. This method uses skin placed markers and multiple cameras to capture the movement of the body. However, recent studies have used Inertial Measurement Units (IMUs) to capture body movements[2]. An IMU consists of 9 sensors, 3 orthogonal accelerometers, angular rate gyroscopes and magnetometers. An IMU is the size of a small match box and has its own power supply, data acquisition and data storage, making it a completely independent system.

IMUs offer numerous advantages advantages over stereophotogrammetry methods. Since they are independent systems, IMUs are not restricted to certain measurement volumes. Furthermore, IMUs experience no hindrance from multiple persons moving close to one another or having direct contact with each other. This makes IMUs the best suitable method to capture the lower body kinematics of team sports such as football. Other advantages IMUs have over stereophotogrammetry methods are a short set-up time, lower purchase costs and less extensive placement methods.

An important difference between IMUs and stereophotogrammetry methods is that stereophotogrammetry methods measure the position of markers on anatomical landmarks, whereas IMUs measure linear acceleration, angular velocity and the magnetic field, which are used to determine the orientation of the IMU. Therefore both methods require different calibration and data processing techniques. Because of these differences, there is also a difference in outcome for both methods. In the last decade multiple studies have validated IMUs with stereophotogrammetry for whole body kinematics[3], lower body kinematics during gait[4][5], lower body kinematics during dynamic movements[6][7] and upper body kinematics[8][9]. Overall these studies showed promising results for the IMUs with a high correlation with the stereophotogrammetry. However, a relative error between both methods was present in all studies and ranged from 2-14 deg RMSE. This relative error has three important sources: the definition of the body frames, soft tissue artefacts and the orientation filter.

B. Definition Body Frames

To convert measurements into relevant body frames a biomechanical model is used. Stereophotogrammetry methods can use a model based on anatomical landmarks and anthropometric measurements to define body frames. IMUs on the other hand have their own local coordinate system. Because an IMU can be placed at any arbitrary point on a segment, in any arbitrary orientation, it is necessary to transform the local coordinate system of the IMU to the body frame of the segment. This sensor-body alignment can be done with postural calibrations[10][11][12][13] or a combination of postural and movement calibrations[14][15]. The global coordinate system of an IMU is defined with use of the magneto- and accelerometers. One axis is defined opposite to the gravity and an auxiliary axis is in the direction of the magnetic north. With these two axes an orthogonal coordinate system is created. Most calibration techniques assume that a body part is parallel with the gravity in the neutral standing pose. Therefore, in this pose the longitudinal axis and the transverse plane of the body segment and the sensor are aligned. The next step of a calibration process requires either a pose or movement in which the desired body segments move only in either the saggital or frontal plane. The axis over which this movement, or change between poses, has happened can be used to define a second axis and subsequently a third orthogonal axis can be calculated.

The study by Robert-Lachaine et al. (2017)[10] validated different IMU biomechanical models with an optoelectronic system. The body frames were defined with an error of up to 7.0 deg RMSE of the joint euler angles of the lower extremities. Other studies[11][12][14] found similar errors. This error can be caused by the fact that a body segment is not completely parallel to the gravity during a standing pose. A second source of error is the fact that human subjects have great difficulty to perform a motion around a single axis. Even when the skeletal system performs a perfect motion around a single axis, the sensor or marker can move relative to the bone. This third source of error for the definition of the body frames is known as the Soft Tissue Artefact and is also a source of error during the actual measurements.

C. Soft Tissue Artefacts

The Soft Tissue Artefact (STA) is defined as the error caused by the relative motion between the bone and the skin. STA is the biggest source of error in the field of human motion analysis[16]. STA varies between subjects because of its dependence on: fat percentage, muscle size, limb length and skin impedance. Furthermore, the STA within subjects also varies because of its dependence on: marker/sensor location, marker/sensor mass, marker/sensor placement method and type of experimental activity[17][18][19][20][21]. STA has both high and low frequent behaviour. The high frequent behaviour is caused by inertia effects at moments of impact and high acceleration. The low frequent behaviour is caused by the stretching or sliding of the skin due to segment rotations or muscle contractions. Human movement studies deal with STA by minimizing the STA during either the data acquisition or the data processing. During the data acquisition, STA minimization can be done by adjusting participant selection, optimizing sensor location, decreasing sensor mass, optimizing sensor placement method or optimizing the experimental movement. During the data processing, STA can be minimized with filtering techniques. The high frequent behaviour of STA has a higher frequency than the actual movements of the body and can thus be filtered out with a low-pass filter.
Both stereophotogrammetry and IMU suffer from STA. However, stereophotogrammetry is expected to be less vulnerable to STA because it measures position. If the position of markers on anatomical landmarks are influenced by STA, the modeled orientation of the body segment is only slightly influenced. An IMU on the other hand measures acceleration, angular velocity and magnetic field strength. Therefore, if the motion of the IMU is influenced by STA, the modeled orientation of the body segment is strongly influenced. However, since STA quantification is difficult and has so far been limited to small scale, low activity studies[22], no studies have quantified the STA of IMUs. For stereophotogrammetry methods the STA is largest on the thigh and has been quantified for up to 32 mm translation[23]. This could result in a 20 deg error. However, when markers are placed on bony landmarks, STA can be strongly mitigated to sub degree values [17][19][21].

D. Orientation Filter

To find the orientation of a body segment, the measurements of the rate gyroscopes of an IMU have to be integrated. However, due to integration drift, the computed orientation would suffer from large errors within seconds. Therefore the measurements of the rate gyroscopes have to be optimized. This can be done with the use of accelerometers and magnetometers. Since both these sensors always have a measurement in a constant direction (gravity for the accelerometers and the magnetic north for the magnetometers) they can be combined with the measurements of the rate gyroscopes to measure orientation accurately. To combine these measurements an orientation filter, or sensor fusion algorithm is used. A study by Ludwig et al. (2018)[24] compared a Kalman, Mahony and Madgwick orientation filter. All filters had comparable errors but the Madgwick orientation filter required far less computational power. The Madgwick orientation filter has a single adjustable filter gain depended on the maximum angular velocity of the rate gyroscopes and the trust in the accelerometers and magnetometers. The Madgwick orientation filter has an reported static error of 0.6 deg RMSE and a dynamic error of 0.8 deg RMSE[25]. However, in this study the dynamic trial consisted of rotating the IMU by hand, resulting in very small accelerations.
For the orientation filter to function properly, the axis of the accelerometers, gyroscopes and magnetometers have to be aligned. Since the sensors are all separate pieces of hardware within the IMU, this is not automatically the case. Another important notion is that all sensors of an IMU have noise and a bias. For the coordinate systems of all sensors to be aligned with each other and for the compensation of the bias in each sensor, a sensor calibration procedure is necessary[26][27].
An assumption the orientation filter makes is that the gravity and magnetic north have a constant direction. However, a study by De Vries et al. (2009)[28] has shown that in a laboratory environment magnetic distortions can be present. These magnetic distortions can lead to an error of 21 deg[29]. Furthermore, if the IMU experiences substantial linear accelerations, the accelerometers no longer measure a vector aligned with the gravity. This misalignment error can be minimized by optimizing the filter gain and will be of importance for movements with high accelerations.

E. Problem Analysis, Goal and Hypothesis

Multiple studies have been performed to validate IMUs with stereophotogrammetry[3][4][6][7][8]. Although some of these studies have differentiated their results between different sources of errors, to the best of our knowledge, no study has been performed separating the error of IMUs in the definition of the body frames, the STA and the orientation filter. Especially the STA has never been quantified for IMUs. Furthermore, current studies have examined the different sources of error during a low level activity, like gait. No study has examined the different sources of error for a explosive, dynamic activity, like football. To increase the accuracy of IMUs for capturing lower-body kinematics during football activities, the sources of error have to be

quantified.
The goal of this study is to quantify the different sources of error of human motion analysis with IMUs. Also, to compare different calibration techniques, movements and movement intensities and examine their influence on the different sources of error. The quantification of these errors can provide a necessary insight for all human motion analysis studies using IMUs and would allow for the optimization of error reduction techniques.

It was hypothesized that a calibration movement for which the subject continuously has two contact points with the ground outperforms a calibration movement that has one contact point with the ground. Since for a movement with only one contact point the center of mass has to be moved above the contact point, it is assumed that this movement is executed less precise. The STA is expected to be the largest for the IMUs on the thigh since on this body segment most soft tissue is present. The STA is also expected to increase with movement intensity due to inertia effects. The error of the orientation filter is expected to be largest for the IMUs on the shanks, since these experience the highest linear acceleration and angular velocity. Also, it is expected that the error of the orientation filter increases with movement intensity due to higher linear accelerations and angular velocities.

II. METHOD

A. Subjects and Instrumentation

10 male subjects (mean $\pm$ std: age [y] 22.6 $\pm$2.2, height [cm] 180.6 $\pm$8.7, weight [kg] 70.3 $\pm$9.8) participated in the study. All subjects were active football players with at least five years experience and had their right leg as their preferred leg of shooting. All subjects signed an informed consent in accordance with the Declaration of Helsinki and approved by the ethics committee of the VU Amsterdam. No subjects had any injury at the time of testing. The study was conducted at the Royal Dutch Football Association (KNVB) Campus.

Subjects were equipped with five IMUs (MPU-9150, Invensense, SanJose, CA, USA). The IMUs were placed on the left and right thigh, left and right shank and on the pelvis, see Fig. 1. Data was gathered at 500 Hz and logged on a SD card inside the IMU, allowing for offline analysis.

Sixteen retro-reflective markers were placed on the following anatomical landmarks: the anterior and posterior superior iliac spines, the posterior side of the thighs halfway the length hip to knee, the medial and lateral femoral epicondyles, the anterior side of each shank halfway the length knee to ankle and the medial and lateral malleoli, see Fig. 1. The location of the markers was captured at 250 Hz with cameras of the Vicon Optoelectronic system (Vicon V5 cameras, Vicon Motion Systems Ltd., Oxford, UK).

A Rigid Marker Cluster (RMC) is a rigid connection between 4 markers and the IMU[7]. A 3D model was designed in SolidWorks (SolidWorks 2015, Dassault Systèmes, Winchester, Massachusetts, USA) and printed in PLA with an Ultimaker 3D printer, see Fig. 2. The position of these markers was also captured at 250 HZ with the Vicon Optoelectronic system. The local coordinate system of the RMCs is defined so that when an IMU is placed inside the RMC, their coordinate systems are aligned. Because of the rigid IMU-marker connection and the aligned local coordinate systems, no error caused by the definition of the local coordinate system and no STA is present. Therefore the relative error between the IMU and the RMC is caused by the orientation filter.

B. Protocol

The IMUs were turned on and placed in a box with specific IMU fittings, preventing the IMUs from moving relative to each other. The box was tapped on a hard surface to introduce a peak value in the accelerometers. This peak was used to time synchronise all IMUs[30]. The IMUs and markers were fixed to the RMCs with double sided adhesive tape. The RMCs and markers were placed on shaved skin with double sided adhesive tape. Another layer of tape was applied around the markers and over the RMC to ensure a proper connection throughout the whole experiment.

Because the IMUs are placed in different orientations with respect to the body segments, a sensor-body calibration is necessary to construct coordinate systems for each body segment. Three different sensor-body calibrations were performed. All calibration methods had the same first step, a static calibration in the neutral pose. In this position the longitudinal axis of the body segments were assumed to be parallel to gravity and could therefore be defined. The second step of the sensor-body calibration was a movement performed in the saggital plane and could therefore be used to define the frontal axis of the body segments. The third axis of the coordinate systems of the body segments was defined orthogonal to the longitudinal and horizontal axis. The three different sensor-calibration movements were: bow and thigh rise(A), squat(B) and inclined plank(C)[13], see Fig. 3. For the inclined plank movement the subject has to place his hands on an object in front him and move towards this object while keeping his legs an torso in a straight line.

After the sensor-body calibration, three types of movement were executed at three intensities. The nine different trials were: a squat, a squat jump at 50% intensity, a squat jump at 100% intensity, a walk, a run at 50% intensity, a sprint at 100% intensity, a pass, a cross and a shot, all with the right leg. Each trial was repeated eight times. For each trial and for each body segment, three data sets were recorded: the position of the markers on the anatomical landmarks, the position of the markers of the RMCs and the angular velocity, linear acceleration and magnetic field strength of

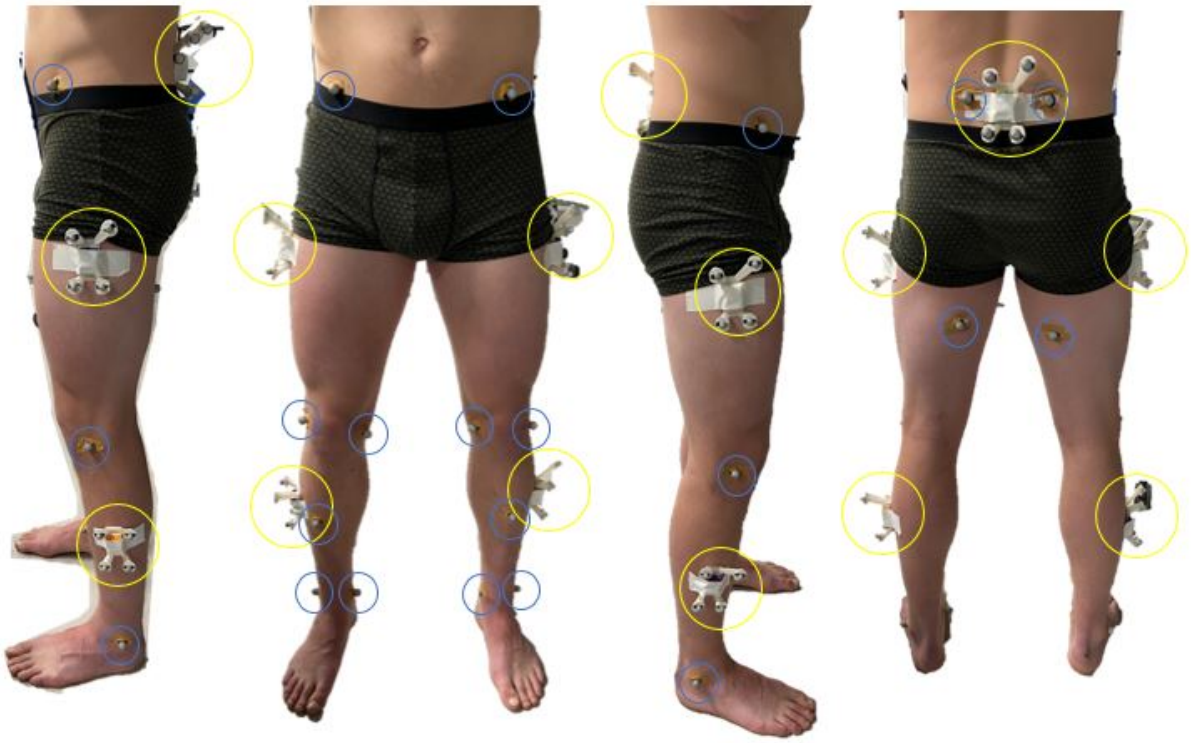

Fig. 1: Subject instrumentation. IMUs were placed in the Rigid Marker Clusters and placed on the left and right thigh, left and right shank and pelvis, yellow circles in the figure. Markers were placed on the following anatomical landmarks: the anterior and posterior superior iliac spines, the posterior side of the thighs halfway the length hip to knee, the medial and lateral femoral epicondyles, theanterior side of each shank halfway the length knee to ankle and the medial and lateral malleoli, blue circles in the figure.

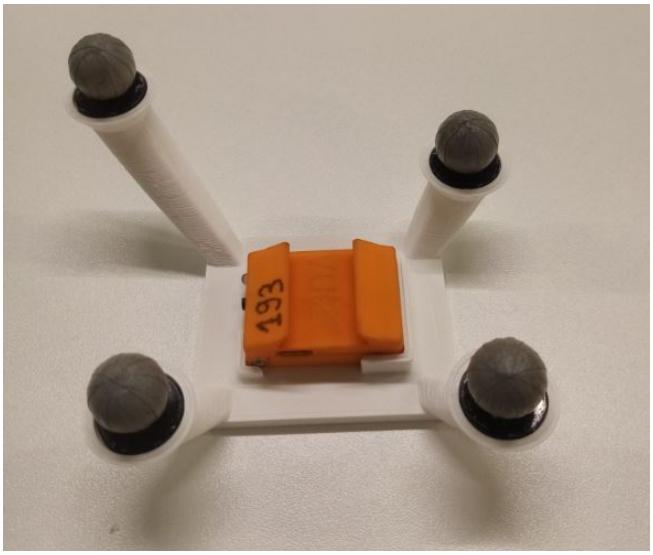

Fig. 2: Rigid Marker Cluster (RMC)[7]

the IMUs.

C. Data Processing

The raw marker position data was processed in Vicon Nexus (version 2.7.3, Vicon Motion Systems Ltd., Oxford, UK). Possible gaps in marker trajectories were filled using Nexus' Woltring gap fill algorithm, the rigid body gap fill and the kinematic gap fill for gaps of a maximum of 0.05, 0.1 and 0.7 seconds, respectively, according to the recommendations by Visual 3D (C-Motion, Inc, Germantown, MD, USA). Of the eight recorded trials, the first five trials without gaps larger than 0.7 seconds were used for further processing. Marker data was exported to Matlab (version 2020a, The MathWorks, Inc., Natick, MA, USA). A low-pass, fourth order Butterworth filter with a cut-off frequency of 8 Hz was applied to all marker trajectories. Based on the markers on the anatomical landmarks, in combination with a measurement of the leg length, body frames were defined for the left and right thigh, left and right shank and the pelvis, based on Cappozzo et al. (1995)[31] and following ISB recommendations[32]. These body frames were named the Anatomical Landmark marker calibrated body frames (AL-mcbf). The markers on the RMC were used to construct a RMC sensor frame (RMC-sf) which aligned with the IMU sensor frame (IMU-sf). Both the orientation of the AL-mcbf and the RMC-sf frames were described as rotation quaternions relative to the global reference frame (GRF) of the Vicon system.

Data from the IMUs were exported to Matlab and down-sampled to 250 Hz to match the frequency of the other data

Fig. 3: Sensor-body calibration movements. Calibration A consists of a neutral pose followed by a bow, right thigh rise and left thigh rise. Calibration B consists of a neutral pose and a squat movement. Calibration C consists of a neutral pose and an inclined plank movement.

sets. Accelerometer and magnetometer data were normalized since only the direction of these quantities was used. Offsets and misalignment in the IMU sensors were compensated for with an IMU-sensor calibration[26][27]. This calibration could be performed offline and after data acquisition. A gradient decent Madgwick algorithm with a filter gain of 0.043[25] was used to compute the orientation of the IMU sensor frame (IMU-sf) relative to the IMU-Reference frame (IRF). The already described sensor-body calibration movements were used to compute the IMU-body frames. The sensor-body calibration procedure was based on Wilmes et al. (2020)[6] and followed the ISB recommendations[32]. Body frames were constructed for each of the different sensor-body calibration movements. These frames were named the IMU sensor calibrated body frames A-C (IMU-scbf(A-C)) based on which calibration movement was used, see equation 1, (${}^{B}_{A}q$ is the rotation quaternion from frame A to frame B, q_t is a time varying rotation quaternion and q is a time invariant rotation quaternion).

$$ {}^{IMU-scbf(A-C)}_{IRF}q_t = {}^{IMU-sf}_{IRF}q_t \otimes {}^{IMU-scbf(A-C)}_{IMU-sf}q \quad (1) $$

To compare the different frames, all frames have to be described relative to the same global frame. The problem of finding the relative orientation between the coordinate frames of different systems is known in the field of robotics as the hand-eye calibration problem[33]. A large compass with markers at both ends was used to determine the direction of the local magnetic field relative to the GRF[25]. Because the IMUs use this direction to determine the IRF, the quaternion between the IRF and GRF could be calculated. This quaternion was then used to describe the IMU-sf and the IMU-scbf(A-C) relative to the GRF, see equation 2 and 3.

$$ {}^{IMU-sf}_{GRF}q_t = {}^{IRF}_{GRF}q \otimes {}^{IMU-sf}_{IRF}q_t \quad (2) $$

$$ {}^{IMU-scbf(A-C)}_{GRF}q_t = {}^{IRF}_{GRF}q \otimes {}^{IMU-scbf(A-C)}_{IRF}q_t \quad (3) $$

Furthermore, to quantify the error of the definition of the body frames, the IMU-sf and RMC-sf were rotated to a marker calibrated body frame, based on a the static trial, see equation 4-7. An overview of all data processing is given, see Fig. 4.

$$ {}^{IMU-sf}_{AL-mcbf}q = \frac{1}{n}\sum_{t=1}^{n}\left(\left({}^{AL-mcbf}_{GRF}q_t \right)^{-1} \otimes {}^{IMU-sf}_{GRF}q_t \right) \quad (4) $$

$$ {}^{IMU-mcbf}_{GRF}q_t = {}^{IMU-sf}_{GRF}q_t \otimes {}^{AL-mcbf}_{IMU-sf}q \quad (5) $$

$$ {}^{RMC-sf}_{AL-mcbf}q = \frac{1}{n}\sum_{t=1}^{n}\left(\left({}^{AL-mcbf}_{GRF}q_t \right)^{-1} \otimes {}^{RMC-sf}_{GRF}q_t \right) \quad (6) $$

$$ {}^{RMC-mcbf}_{GRF}q_t = {}^{RMC-sf}_{GRF}q_t \otimes {}^{RMC-sf}_{AL-mcbf}q \quad (7) $$

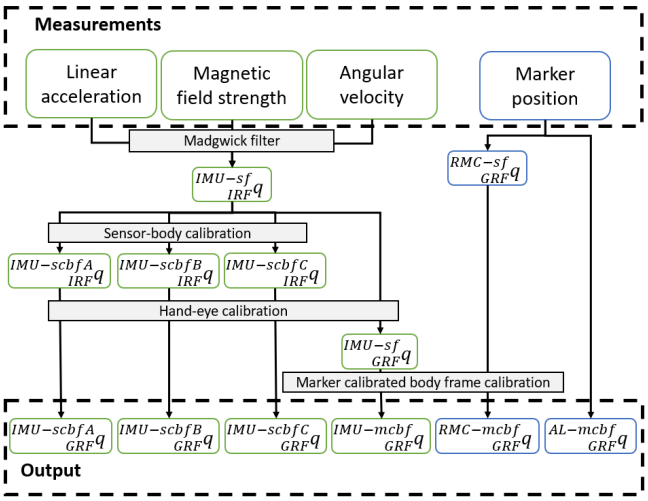

Fig. 4: Flow chart of the data processing. Measurements were converted to rotation quaternions between two frames. IRF = IMU Reference Frame, GRF = Global Reference Frame, IMU-sf = IMU sensor frame, IMU-scbf(A-C) = IMU sensor calibrated body frame A, B and C, RMC-sf = RMC sensor frame, AL-mcbf = Anatomcial Landmarks marker calibrated body frame, IMU-mcbf = IMU marker calibrated body frame and RMC-mcbf = RMC marker calibrated body frame. The sensor-body calibration is based on the different calibration movements(A-C). The hand-eye calibration is based on the marker compass measurement. The marker calibrated body frame calibration is based on a static trial.

D. Data Analysis

After data processing, six different body frames (IMU-scbfA, IMU-scbfB, IMU-scbfC, IMU-mcbf, RMC-mcbf and AL-mcbf) are described relative to the global frame for each body segment. Table I shows the comparisons between the frames that were made.

	frame 1	frame 2	Error
#1	IMU-scbfA	IMU-mcbf	Error definition body frames A
#2	IMU-scbfB	IMU-mcbf	Error definition body frames B
#3	IMU-scbfC	IMU-mcbf	Error definition body frames C
#4	RMC-mcbf	AL-mcbf	STA
#5	IMU-mcbf	RMC-mcbf	Error orientation filter
#6	IMU-mcbf	AL-mcbf	Error orientation filter + STA
#7	IMU-scbfA	AL-mcbf	Total error with calibration A
#8	IMU-scbfB	AL-mcbf	Total error with calibration B
#9	IMU-scbfC	AL-mcbf	Total error with calibration C

TABLE I: Comparisons between the different body frames and the error that the difference in frames describes.

As described in the introduction, there are three main sources of error between IMUs and an optoelectronic system: the definition of the body frames, the soft tissue artefact (STA) and the orientation filter. In comparison #1-3 the same measurements are used to compute the orientation of the body segments. However, since different sensor-body calibration methods are used, the difference in these comparisons is the error caused by the definition of the body frames. In comparison #4 the frames are constructed from measurements of the optoelectronic system and are therefore not influenced by the orientation filter. Furthermore are the frames calibrated to the same body frame. Therefore, because the body frames measured with the RMCs are influenced by STA, the difference in comparison #4 is caused by the STA. In comparison #5, there is a rigid connection between the IMU and the RMC preventing the STA. And because both frames are aligned, no error from the definition of the body frames is present. Therefore the error found in comparison #5 is the error caused by the orientation filter. In comparison #6 measurements form the IMUs are compared to the optoelectronic system and also calibrated to the same body frame. Therefore the difference is the combined error of the orientation filter and the STA. In comparison #7-9 the IMU body frames are calibrated based on the calibration movements(A-C). Therefore the difference in these comparisons include the error caused by the definition of the local frames, the STA and the orientation filter.

Each comparison was described by the rotation quaternion between the two frames. From this quaternion the smallest rotation between the two frames was calculated in degrees. For each trial the RMSD of the smallest angle between the frames was calculated. For each subject the mean over five repetitions of all nine different trials was calculated. Subsequently the mean and STD of the RMSD over all subjects was calculated for each trial and each body segment. A three-way repeated measures ANOVA with Bonferroni post-hoc comparisons were performed to assess the effects of movement type, intensity, and body segment (3 movement types x 3 intensities x 5 segments) on the STA errors, orientation filter errors, the total errors. A Greenhouse-Geisser correction was applied if the assumption of sphericity was not met. The significance level was set at $p < 0.05$ and effect size was calculated as eta squared(η^2).

III. Results

A. Definition Body Frames

Fig. 5 shows the RMSD and STD of the error of the definition of the body frames for calibration A, B and C. The error of the definition of the body frames was constant over time and thus constant for all trials for each subject. No calibration method significantly outperforms the others. The errors ranged between 11.3 and 18.7 deg RMSD. All three calibration methods showed large between subject variability with a STD of up to 8.8 deg.

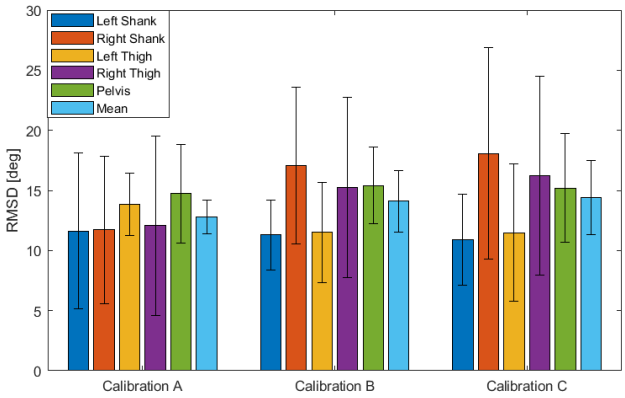

Fig. 5: Error of the definition of the body frames. RMSD of all body segments for the 3 different calibrations, see Fig. 3 for calibration movements.

B. Soft Tissue Artefact

Table II shows the main and interaction effects on the error caused by the STA. Movement type, intensity and segment were all significant main effects. Fig. 6 shows the mean RMSD and STD of the STA for all body segments and for all trials. The RMSD of the STA ranged from 3.8 degrees on the pelvis during the walk trial, to 9.1 degrees on the right thigh during the sprint trial. For the walk, run, cross and shot trial, the STA on both thighs was larger than the STA on the pelvis. However, for the squat trial, the STA on the pelvis was larger than the STA of the shanks. The STA mean overall body segments of the sprint trial was higher than all other trials except the run trial. Fig. 7 shows the error caused by the STA plotted over time for each trial of a typical subject. In the top right corner of each plot the mean RMSD overall body segments and the maximum error are displayed in degrees. It can be seen that the STA is not a constant offset or white noise but that the error is very

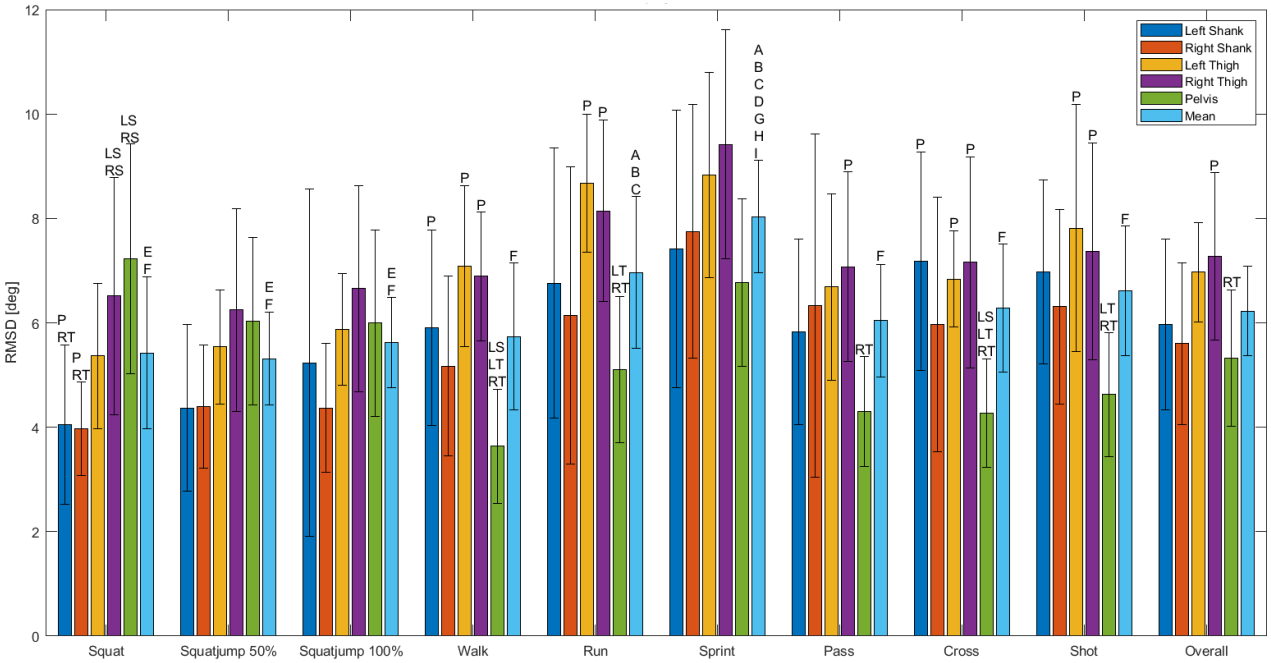

Fig. 6: Error caused by the STA. Mean RMSD and STD for all body segments and all trials. Significant differences within each trial between body segments are displayed by letters above the bar, LS, RS, LT, RT and P mean a significant difference with the left shank, right shank, left thigh, right thigh and pelvis, respectively. Significant differences between trails are display with a letter above the mean bar. A = squat, B = squatjump 50%, C = squatjump 100%, D = walk, E = run, F = sprint, G = pass, H = cross and I = shot.

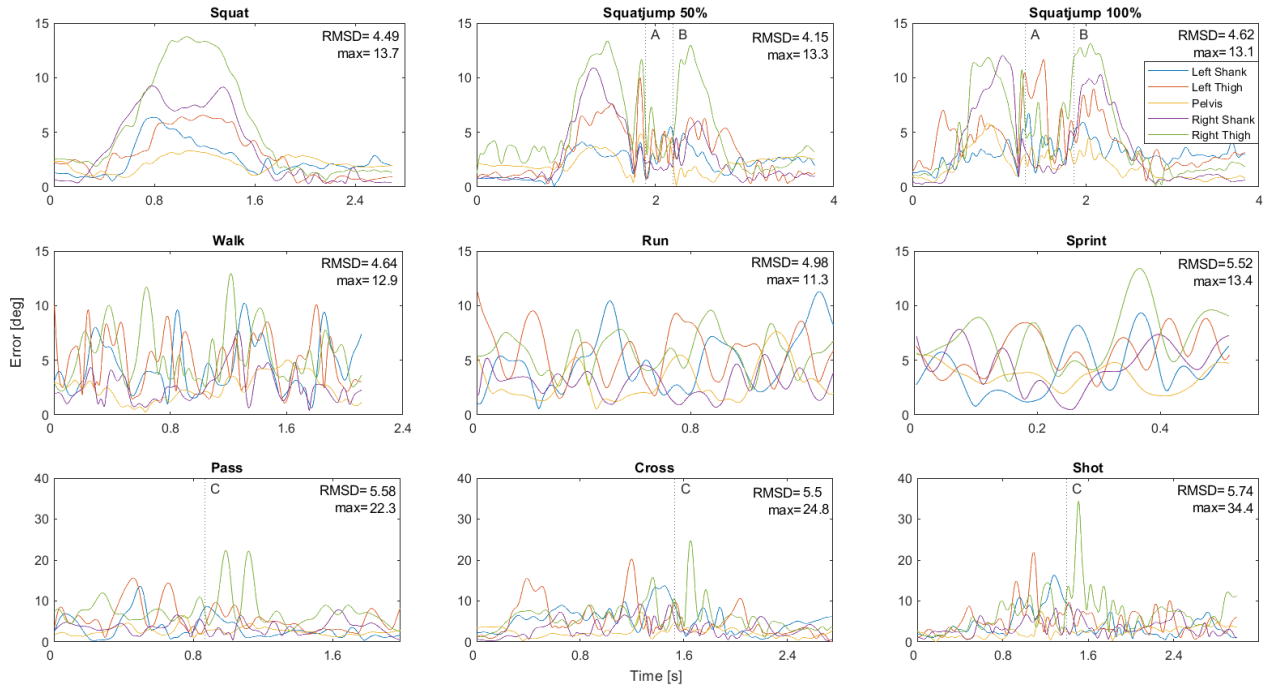

Fig. 7: Error caused by the STA, plotted for each trial over time of a typical subject. In the top right corner of each plot the RMSD overall body segments and maximum error are displayed in degrees. The vertical dashed line represent a specific moment in time: A = push off, B = landing, C = ball contact.

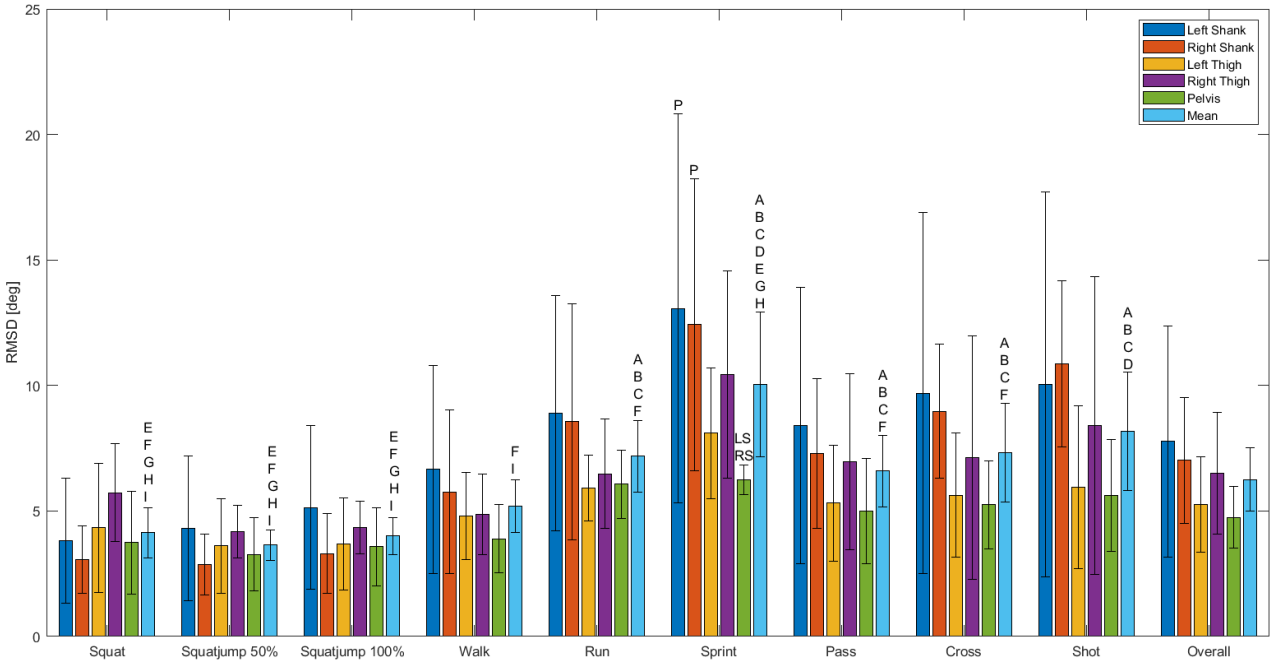

Fig. 8: Error of the orientation filter. Mean RMSD and STD for all body segments and all trials. Significant differences within each trial between body segments are displayed by letters above the bar, LS, RS, LT, RT and P mean a significant difference with the left shank, right shank, left thigh, right thigh and pelvis, respectively. Significant differences between trails are display with a letter above the mean bar. A = squat, B = squatjump 50%, C = squatjump 100%, D = walk, E = run, F = sprint, G = pass, H = cross and I = shot.

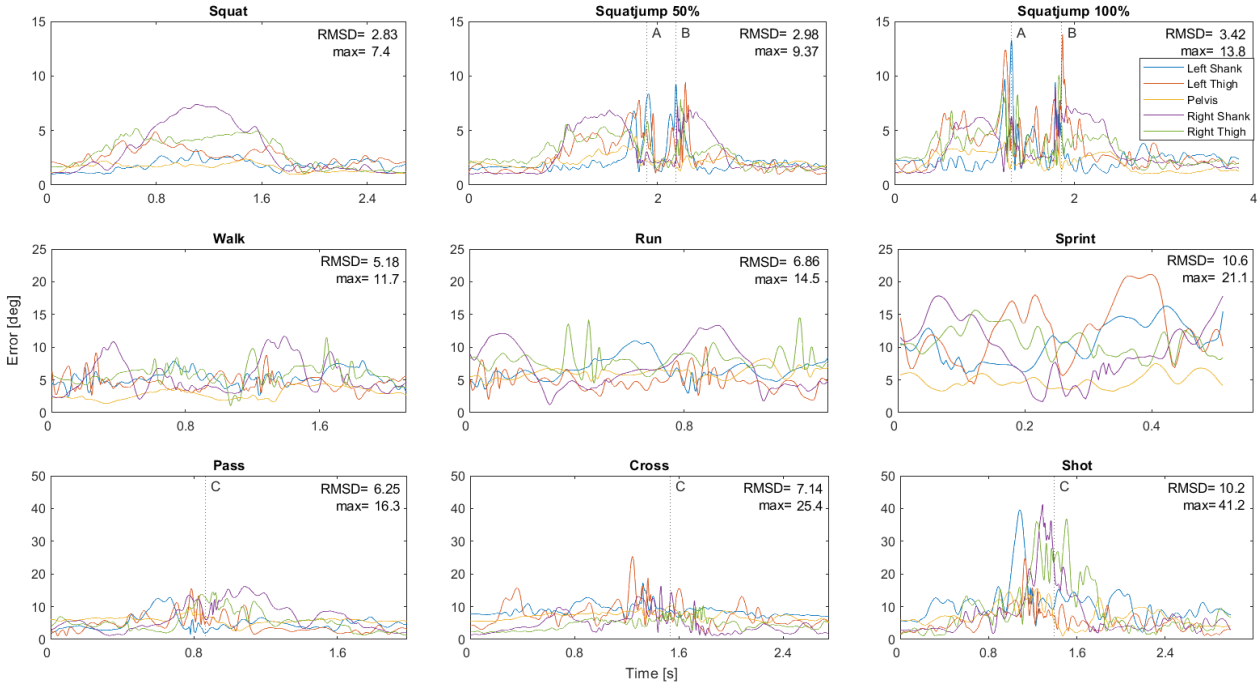

Fig. 9: Error of the orientation filter, plotted for each trial over time of a typical subject. The exact same trails were used in Fig. 7. In the top right corner of each plot the RMSD overall body segments and maximum error are displayed in degrees. The vertical dashed line represent a specific moment in time: A = push off, B = landing, C = ball contact.

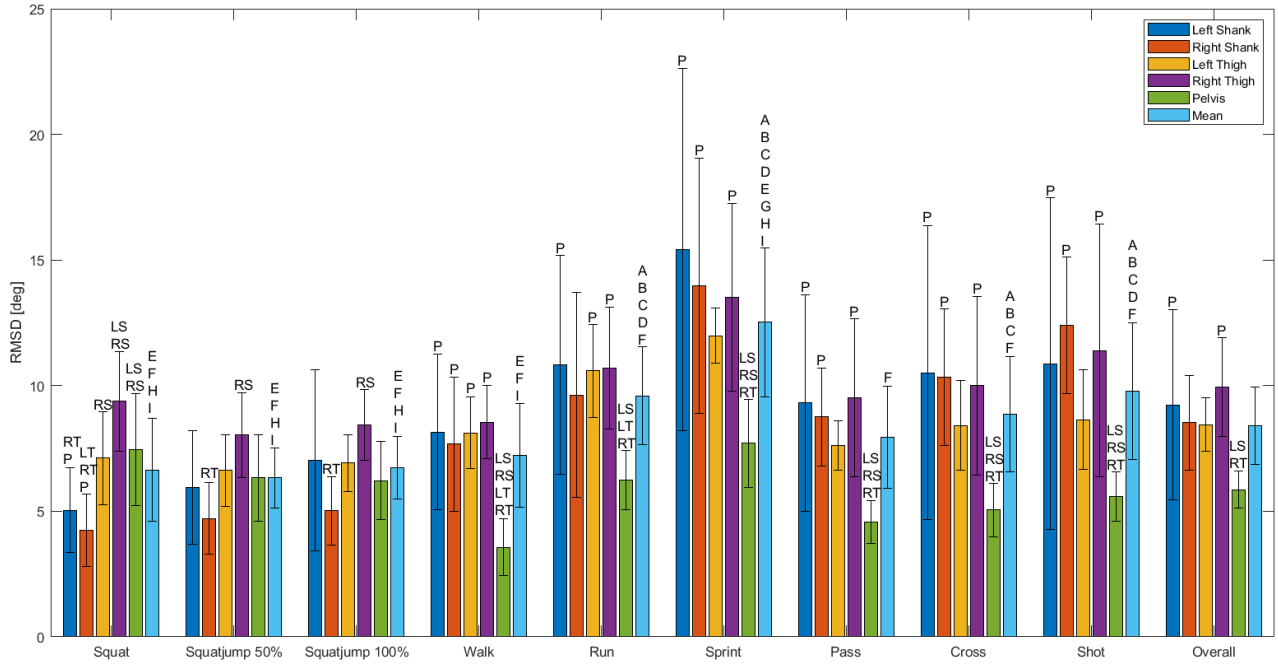

Fig. 10: Combined error of the STA and the orientation filter. Mean RMSD and STD for all body segments and all trials. Significant differences within each trial between body segments are displayed by letters above the bar, LS, RS, LT, RT and P mean a significant difference with the left shank, right shank, left thigh, right thigh and pelvis, respectively. Significant differences between trails are display with a letter above the mean bar. A = squat, B = squatjump 50%, C = squatjump 100%, D = walk, E = run, F = sprint, G = pass, H = cross and I = shot.

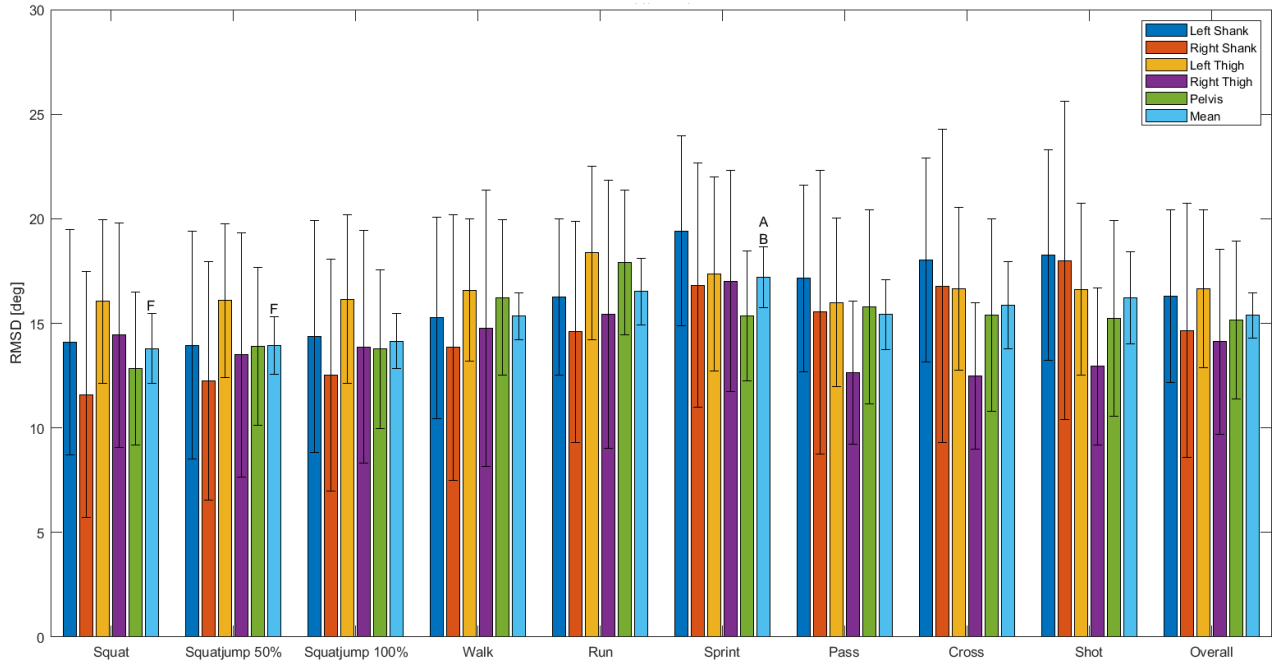

Fig. 11: Total error with sensor-body calibration A. Mean RMSD and STD for all body segments and all trials. Significant differences within each trial between body segments are displayed by letters above the bar, LS, RS, LT, RT and P mean a significant difference with the left shank, right shank, left thigh, right thigh and pelvis, respectively. Significant differences between trails are display with a letter above the mean bar. A = squat, B = squatjump 50%, C = squatjump 100%, D = walk, E = run, F = sprint, G = pass, H = cross and I = shot.

TABLE II: Significance and effect size of main and interaction effect of movement type, intensity and segment on the RMSD of the error caused by the STA, the Orientation Filter and the Total Error. Insignificant effects were denoted with an astrix(*)

	Error STA		Error Orientation Filter		Total Error	
	p	η^2	p	η^2	p	η^2
Movement type	<0.001	0.100	<0.001	0.201	<0.001	0.046
Intensity	<0.001	0.052	<0.001	0.066	<0.001	0.008
Segment	<0.001	0.154	0.018	0.104	0.604*	0.040
Movement type : Intensity	<0.001	0.042	<0.001	0.063	0.046	0.003
Movement type : Segment	<0.001	0.132	0.006	0.055	<0.001	0.038
Intensity : Segment	0.750*	0.004	<0.001	0.019	<0.001	0.008
Movement type : Intensity : Segment	0.001	0.025	0.003	0.012	<0.001	0.009

much time dependent. For the squatting trials, the STA arises during the flexion of the knees, both before push off and after landing for the squatjumps. For the walk, run and sprint trial, the STA shows a cyclic pattern related to the gait cycle. The shooting trials display a spike of the left thigh before ball contact and a spike of the right thigh right after ball contact. The spike before ball contact is caused by the landing of the stance leg, the spike after ball contact by the ball contact and the swing through of the shooting leg. The maximum error in time occurred during the shot trial on the right thigh and was 34.4 degree.

C. Orientation filter

Table II shows the main and interaction effects on the error caused by the orientation filter. Movement type, intensity and segment were all significant main effects. Fig. 8 shows the mean RMSD and STD of the error caused by the orientation filter for all body segments and for all trials. The RMSD of the error caused by the orientation filter ranged from 3.0 degrees on the left shank during the squat trial to 12.7 degrees on the left shank during the sprint trial. For the sprint trial, the error of the orientation filter was larger on both shank than on the pelvis. The mean error of all body segments combined was lower for the squatting trails compared to all other trials, except the walking trial. The mean error overall body segments was for the sprint trial larger than all other trials, except the shot trail. Fig. 9 shows the error caused by the orientation filter plotted over time for the same subject and the same trials as in Fig. 7. It can be seen that the error caused by the orientation filter is highly time dependent. The error over time consists of a constant offset of around 1 degree, some high frequent behaviour around moments of impact and some low frequent behaviour related to movement. For the squatting trials, the error of the orientation filter arises during the flexion of the knees, both before push off and after landing for the squatjumps. For the walk, run and sprint trial, the error of the orientation filter shows a cyclic pattern related to the gait cycle. The shooting trials display high frequent behaviour around the moment of ball contact. A relationship between movement intensity and maximum error in time is visibly. The maximum error in time occurred during the shot trial on the right shank and was 41.2 degrees.

D. Combined Error STA and Orientation Filter

Fig. 10 shows the mean RMSD and STD of the combined error of the STA and the orientation filter for all body segments and for all trials. The RMSD of the combined error ranged from 3.5 degrees on the pelvis during the walk trial to 15.4 degrees on the left shank during the sprint trial. For running and shooting trials the combined error was lower on the pelvis than on other bodysegments. The mean error overall bodysegments combined was higher for the sprint trail compared to all other trials.

E. Total Error

Fig. 11 shows the mean RMSD and STD of the total error with sensor-body calibration A for all bodysegments and for all trials. The RMSD of the total error ranged from 11.6 degrees on the right shank during the squat trails to 19.4 degrees on the left shank during the sprint trail. Fig. 12 shows the mean RMSD and STD for each of the sources of error, for the combined error of the STA and the orientation filter and for the total error, averaged over all trials. To reduce the amount of displayed data the error of the definition of the body frames and the total error is only displayed for sensor-body calibration A.

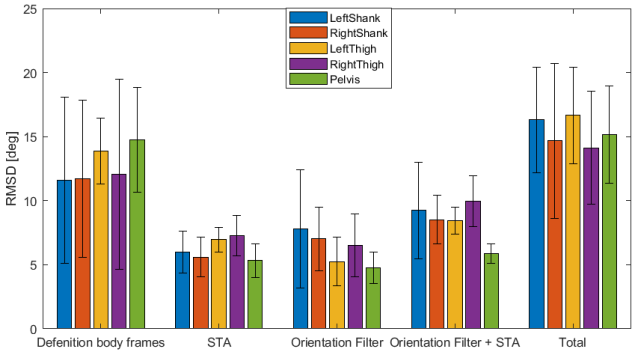

Fig. 12: RMSD and STD for each of the sources of error and total error, for all body segments, mean overall trials. The error of the definition of the body frames and the total error is displayed for calibration A.

IV. Discussion

The goal of this study was to quantify the different sources of error of an IMU during a football activity and to study the influence of different sensor-body calibration methods, different movements and movement intensities on

the sources of error. The sources of error were quantified by comparing the IMUs against an optoelectronic system. It should be noted that the optoelectronic system is not a golden standard in all cases and therefore the results were described by RMSD instead of RMSE. Another important notion is that because the goal of this study was to get a complete insight in the different sources of error, no error minimization techniques, like a low-pass filter, were used on the IMU data. In current literature this is not the case. Furthermore, unlike current literature, this study described the orientation of body segments instead of joint angles. This choice was also made to get a greater insight in the different sources of error.

A. Definition Body Frames

The definition of the body frames was the largest source of error for the IMUs. Unlike hypothesized, the type of calibration movement did not have a significant influence on the definition of the body frames. However, the high between subjects variability shows that there are other factors that cause a difference. This difference could arbitrarily be attributed to either the IMUs or the optoelectronic system, depending on which one is chosen as the golden standard. The high between subjects variability could be caused by inconsistent execution of the calibration movements, or by inconsistent anthropometry or marker placement, which would influence the marker calibrated body frames.
A study by Robert-Lachaine et al. (2017)[10] also compared the defined body frames of IMUs with an optoelectonic system. The results ranged from 2.5 - 7.0 deg RMSE of the joint Euler angles of the lower extremities. This considerably smaller error could be explained by the fact that this study used the Xsense MVN model. The MVN model uses a combination of static postures and anthropometric measures to define body frames[34]. Furthermore, the study by Robert-Lachaine et al. (2017)[10] used not only leg length but also pelvic width and depth to calculate the marker calibrated body frames. It is also important to distinguish between joint angles and body segment orientations. In the results of the current study, the error of the definition of the body frames of the left shank and thigh and right shank and thigh were very similar. Dependent on the direction of these errors, these could result in smaller errors of the knee joint angle.
The used method in this study was able to quantify the error of the definition of the body frames. The definition of the body frames with IMU could possibly be improved by using models, like the Xsense MVN model, that incorporate antropometric measures. However, the great advantage of IMUs is their ease of use, easy placement method and short set-up time. Therefore, each specific application should make a trade-off between accuracy of the definition of the body frames and practicality.

B. Soft Tissue Artefact

As was hypothesized, the STA depends on type of movement, movement intensity and body segment. However, the variability in the results was quite large. But since the within subject variability was relative small, this variability is caused by differences between subjects (the results of a single subject are display in Appendix I, see Fig. 13.). These between subjects factors could be fat percentage, muscle size but also the placement method.
Fig. 7 shows that the method of this study was also able to analyse the STA over time. High frequent STA was seen at moments of impact, like the landing of the squat jumps and around the moment of ball contact for the shooting trials. However, especially for the squat trials, the range of motion had a much larger influence on the RMSD of the STA. This part of the STA is caused by skin sliding and is related to the flexion or extension of a joint close to the IMU. This can be seen in Fig. 6 by the high STA of the pelvis during the squat trials, during which there is lower back flexion. In all other trails there is little to non lower back flexion and thus less STA on the pelvis.
A limitation of the current method is that the STA is quantified relative to an optoelectronic system, of which the markers also suffer from STA. Golden standard STA quantification techniques require either the surgical placement of bone pins[35] or the use of medical imaging techniques, like fluoroscopy[19]. However, these techniques are highly unsuitable for dynamic activities. As a consequence, there is no available literature regarding STA in dynamic sports activities. Since the markers of the optoelectronic system are placed on bony landmarks, and the IMUs somewhere on the middle of a segment, the relative STA between the two systems was assumed to be a good approximation of the absolute STA of the IMUs. Another limitation of the current method is that the IMUs are placed in the RMCs. This increases the mass of the object fixated on the skin and because part of the STA is caused by inertia, the STA will increase with increasing sensor/marker mass.
Current study is the first study to quantify the STA during dynamic activities and the first study to quantify the STA of IMUs. The used method was able to prove the dependence of STA on movement type, movement intensity and body segment. However, the noted limitations should be taken into consideration when interpreting the absolute values of the results. The low within subject variability does indicate good repeatability of the method. Therefore current method is suitable to study the different factors that influence STA.

C. Orientation filter

The hypothesis that the error of the orientation filter increased with movement intensity was only partially proven by the mean RMSD of the sprint trail being higher that that of the walk and run trial. Furthermore, the hypothesis that the error of the orientation filter would be highest on the shanks was only significantly proven during the sprint trail. This was mainly caused by the high variability in the results. However, the within subject variability was much lower (the results of a single subject are displayed in Appendix I, see Fig. 14.). This indicates that the high variability is caused by between subject factors. The main factor is expected to be the use of different IMUs. Although all IMUs were both

initialized and calibrated in the same way, a difference in performance was noticed.
In Fig. 9 the error caused by the orientation filter could be split up in a constant offset, low frequent behaviour and high frequent behaviour. The constant offset is expected to be caused by the hand-eye calibration, which converted the quaternions to be described relative to the global reference frame instead of relative to the IMU reference frame. After turning the IMUs on they initialize. During this initialization the IMU reference frame is defined, based on measurements of the accelerometers and magnetometers. If the measurements of the magnetometers during initialization do not completely agree with the measurement of the marker compass used for the hand-eye calibration, a constant error will be present. The high frequent behaviour of the error of the orientation filter is expected to be caused by moments of impact, like landing after a squatjump or around the moment off ball contact. During these moments the body segments undergo substantial acceleration, making the direction of the resultant acceleration measured by the accelerometers no longer aligned with gravity. The low frequent behaviour of the error of the orientation filter could have different causes including: misalignment of the sensors of the IMU, a bias in a sensor not compensated for by calibration, noise in the sensors or distortions in the local magnetic field.
A study by Cavallo et al.(2014)[36] used a robotic arm to quantify the error of different orientation filters. For slow rotations (18 deg/s) the Madgwick filter had an error of 5.13 degrees RMSE and 7.07 degrees RMSE for fast rotations (45 deg/s). Since in this study the IMU was only rotated, the influence of linear accelerations was not captured. Furthermore, during the sprint trials angular velocities of up to 1000 deg/s were measured and thus of a far larger magnitude than the study by Cavallo et al.(2014)[36]. Another difference with the current study is that a robotic arm was used as golden standard instead of an optoelectronic system. At dynamic moments of impact and high accelerations, there were gaps in the marker data, which were filled using gap fill algorithms. Especially for dynamic movements, the use of these gap fill algorithms, but also the use of low pass filters, could lead to a reduction of the actual peak orientations. However, based on the low within subject variability and the agreement in magnitude with previous studies, the current method has proved to be able to quantify the error caused by the orientation filter.

D. Combined Error STA and Orientation Filter

The combined error of the STA and the orientation filter can be seen as the error cause by the difference in technology between IMUs and the optoelectronic system. The RMSD of the combined error was in all cases higher than the two separate errors and was approximately the square root of the square of the separate errors. This implies that there is little overlap in the direction of the errors.
A study by Robert-Lachaine et al. (2017)[10] also quantified the error due to technology of IMUs with an optoelectronic system. The experiment consisted of picking up boxes and moving them from one table to another. The results were reported in the RMSE of the joint euler angles and ranged from 1.9 to 7.3 degrees for the lower extremities. These lower errors can be explained by the difference in experimental setup. Since the subjects only had to move from one table to another there were very little dynamics in the lower extremities. Furthermore, a clear distinction has to be made between joint euler angles and the smallest rotation between two body segments when comparing results.

E. Total Error

The total error captured the combined effect of each of the three individual errors. Also, the combined effect of the STA and the error caused by the orientation filter was quantified. The combined effect was approximately the square root of the square of the individual errors, for both the combined effect of the STA and orientation filter and for the total error. This implies that the individual errors are roughly independent of one another.
A study by Wilmes et al.(2020)[6] validated IMUs with an optoelectronic system during dynamic football activities. Overall trails, an error of 5.3 degrees RMSD was reported for the knee and 8.0 degrees RMSD for the hip. These lower results are expected to be caused by the use of filter techniques on the IMU data. In the current study no filtering techniques were used to get insight in the complete error caused by the different sources. Another difference is the use of joint angles instead of segment orientations.

V. Conclusion and Recommendations

This study quantified the different sources of error of human motion analysis with IMUs. During dynamic football activities, the errors of definition of the body frames ranged 11.3 to 18.7 deg RMSD, the STA errors ranged 3.8 to 9.1 deg RMSD, and the error caused by the orientation filter ranged 3.0 to 12.7 deg RMSD. Type of movement, movement intensity and body segment were found to have a significant influence on the errors. Future studies should take these errors into account when using IMUs for human motion analysis. Furthermore, both raw data and data processing scripts of the current study were openly published to give other researchers the opportunity to optimize their own data processing methods and to quantify the performance of different data processing methods.

Data Availability

The data and Matlab scripts for the data processing steps that support the findings of this study are openly available in Zenedo at http://doi.org/10.5281/zenodo.6610795.

Acknowledgements

The author would like to thankfully acknowledge the Dutch Royal Football Association (KNVB) for facilitating the research programme by giving access to their research facilities.

REFERENCES

[1] Vasconcelos, M., Tavares, J. (2008). Human Motion Analysis: Methodologies and Applications. Conference Proceedings of 8th International Symposium on Computer Methods in Biomechanics and Biomedical Engineering. Porto, Portugal

[2] Lopez-Nava, I. H., Munoz-Melendez, A. (2016). Wearable Inertial Sensors for Human Motion Analysis: A Review. IEEE Sensors Journal, 16(22), 7821–7834. https://doi.org/10.1109/jsen.2016.2609392

[3] Robert-Lachaine, X., Mecheri, H., Larue, C., Plamondon, A. (2016). Validation of inertial measurement units with an optoelectronic system for whole-body motion analysis. Medical Biological Engineering Computing, 55(4), 609–619. https://doi.org/10.1007/s11517-016-1537-2

[4] Peruzzi, A., Della Croce, U., Cereatti, A. (2011). Estimation of stride length in level walking using an inertial measurement unit attached to the foot: A validation of the zero velocity assumption during stance. Journal of Biomechanics, 44(10), 1991–1994. https://doi.org/10.1016/j.jbiomech.2011.04.035

[5] Leardini, A., Lullini, G., Giannini, S., Berti, L., Ortolani, M., Caravaggi, P. (2014). Validation of the angular measurements of a new inertial-measurement-unit based rehabilitation system: comparison with state-of-the-art gait analysis. Journal of NeuroEngineering and Rehabilitation, 11(1), 136. https://doi.org/10.1186/1743-0003-11-136

[6] Wilmes, E., de Ruiter, C. J., Bastiaansen, B. J. C., Zon, J. F. J. A. van, Vegter, R. J. K., Brink, M. S., … Savelsbergh, G. J. P. (2020). Inertial Sensor-Based Motion Tracking in Football with Movement Intensity Quantification. Sensors, 20(9), 2527. https://doi.org/10.3390/s20092527

[7] Teufl, W., Miezal, M., Taetz, B., Fröhlich, M., Bleser, G. (2019). Validity of inertial sensor based 3D joint kinematics of static and dynamic sport and physiotherapy specific movements. PLOS ONE, 14(2), e0213064. https://doi.org/10.1371/journal.pone.0213064

[8] Morrow, M. B., Lowndes, B., Fortune, E., Kaufman, K. R., Hallbeck, M. S. (2017). Validation of Inertial Measurement Units for Upper Body Kinematics. Journal of Applied Biomechanics, 33(3), 227–232. https://doi.org/10.1123/jab.2016-0120

[9] Bergamini, E., Guillon, P., Camomilla, V., Pillet, H., Skalli, W., Cappozzo, A. (2013). Trunk Inclination Estimate During the Sprint Start Using an Inertial Measurement Unit: A Validation Study. Journal of Applied Biomechanics, 29(5), 622–627. https://doi.org/10.1123/jab.29.5.622

[10] Robert-Lachaine, X., Mecheri, H., Larue, C., Plamondon, A. (2017). Accuracy and repeatability of single-pose calibration of inertial measurement units for whole-body motion analysis. Gait Posture, 54, 80–86. https://doi.org/10.1016/j.gaitpost.2017.02.029

[11] Morton, L., Baillie, L., Ramirez-Iniguez, R. (2013). Pose calibrations for inertial sensors in rehabilitation applications, 2013 IEEE 9th International Conference on Wireless and Mobile Computing, Networking and Communications (WiMob), Lyon, 2013, pp. 204-211, doi: 10.1109/WiMOB.2013.6673362.

[12] Palermo, E., Rossi, S., Marini, F., Patanè, F., Cappa, P. (2014). Experimental evaluation of accuracy and repeatability of a novel body-to-sensor calibration procedure for inertial sensor-based gait analysis. Measurement, 52, 145–155. https://doi.org/10.1016/j.measurement.2014.03.004

[13] Teufl, W., Lorenz, M., Miezal, M., Taetz, B., Fröhlich, M., Bleser, G. (2018). Towards Inertial Sensor Based Mobile Gait Analysis: Event-Detection and Spatio-Temporal Parameters. Sensors, 19(1), 38–58. https://doi.org/10.3390/s19010038

[14] Favre, J., Aissaoui, R., Jolles, B. M., de Guise, J. A., Aminian, K. (2009). Functional calibration procedure for 3D knee joint angle description using inertial sensors. Journal of Biomechanics, 42(14), 2330–2335. https://doi.org/10.1016/j.jbiomech.2009.06.025

[15] de Vries, W. H. K., Veeger, H. E. J., Cutti, A. G., Baten, C., van der Helm, F. C. T. (2010). Functionally interpretable local coordinate systems for the upper extremity using inertial magnetic measurement systems. Journal of Biomechanics, 43(10), 1983–1988. https://doi.org/10.1016/j.jbiomech.2010.03.007

[16] Peters, A., Galna, B., Sangeux, M., Morris, M., Baker, R. (2010). Quantification of soft tissue artifact in lower limb human motion analysis: A systematic review. Gait Posture, 31(1), 1–8. https://doi.org/10.1016/j.gaitpost.2009.09.004

[17] Kuo, M.-Y., Tsai, T.-Y., Lin, C.-C., Lu, T.-W., Hsu, H.-C., Shen, W.-C. (2011). Influence of soft tissue artifacts on the calculated kinematics and kinetics of total knee replacements during sit-to-stand. Gait Posture, 33(3), 379–384. https://doi.org/10.1016/j.gaitpost.2010.12.007

[18] Cappello, A., Stagni, R., Fantozzi, S., Leardini, A. (2005). Soft Tissue Artifact Compensation in Knee Kinematics by Double Anatomical Landmark Calibration: Performance of a Novel Method During Selected Motor Tasks. IEEE Transactions on Biomedical Engineering, 52(6), 992–998. https://doi.org/10.1109/tbme.2005.846728

[19] Gao, B., Conrad, B., Zheng, N. (2007). Comparison of skin error reduction techniques for skeletal motion analysis. Journal of Biomechanics, 40, S551. https://doi.org/10.1016/s0021-9290(07)70541-9

[20] Andersen, M. S., Damsgaard, M., Rasmussen, J., Ramsey, D. K., Benoit, D. L. (2012). A linear soft tissue artefact model for human movement analysis: Proof of concept using in vivo data. Gait Posture, 35(4), 606–611. https://doi.org/10.1016/j.gaitpost.2011.11.032

[21] Garling, E. H., Kaptein, B. L., Mertens, B., Barendregt, W., Veeger, H. E. J., Nelissen, R. G. H. H., Valstar, E. R. (2007). Soft-tissue artefact assessment during step-up using fluoroscopy and skin-mounted markers. Journal of Biomechanics, 40, S18–S24. https://doi.org/10.1016/j.jbiomech.2007.03.003

[22] Cereatti, A., Bonci, T., Akbarshahi, M., Aminian, K., Barré, A., Begon, M., … Camomilla, V. (2017). Standardization proposal of soft tissue artefact description for data sharing in human motion measurements. Journal of Biomechanics, 62, 5–13. https://doi.org/10.1016/j.jbiomech.2017.02.004

[23] Rouhandeh, A., Joslin, C., Zhen Qu, Yuu Ono. (2014). Non-invasive assessment of soft-tissue artefacts in hip joint kinematics using motion capture data and ultrasound depth measurements. 2014 36th Annual International Conference of the IEEE Engineering in Medicine and Biology Society, 1–2. https://doi.org/10.1109/embc.2014.6944585

[24] Simone A. Ludwig, Kaleb D. Burnham, Antonio R. Jiménez, and Pierre A. Touma "Comparison of attitude and heading reference systems using foot mounted MIMU sensor data: basic, Madgwick, and Mahony", Proc. SPIE 10598, Sensors and Smart Structures Technologies for Civil, Mechanical, and Aerospace Systems 2018, 105982L (27 March 2018); https://doi-org.tudelft.idm.oclc.org/10.1117/12.2296568

[25] Madgwick, S. O. H., Harrison, A. J. L., Vaidyanathan, R. (2011). Estimation of IMU and MARG orientation using a gradient descent algorithm. 2011 IEEE International Conference on Rehabilitation Robotics, 1–32. https://doi.org/10.1109/icorr.2011.5975346

[26] Tedaldi, D., Pretto, A., Menegatti, E. (2014). A robust and easy to implement method for IMU calibration without external equipments. 2014 IEEE International Conference on Robotics and Automation (ICRA), 3042–3049. https://doi.org/10.1109/icra.2014.6907297

[27] Kok, M., Schon, T. B. (2016). Magnetometer Calibration Using Inertial Sensors. IEEE Sensors Journal, 16(14), 5679–5689. https://doi.org/10.1109/jsen.2016.2569160

[28] de Vries, W. H. K., Veeger, H. E. J., Baten, C. T. M., van der Helm, F. C. T. (2009). Magnetic distortion in motion labs, implications for validating inertial magnetic sensors. Gait Posture, 29(4), 535–541. https://doi.org/10.1016/j.gaitpost.2008.12.004

[29] Robert-Lachaine, X., Mecheri, H., Larue, C., Plamondon, A. (2017b). Effect of local magnetic field disturbances on inertial measurement units accuracy. Applied Ergonomics, 63, 123–132. https://doi.org/10.1016/j.apergo.2017.04.011

[30] de Ruiter, C. J., van Dieën, J. H. (2019). Stride and Step Length Obtained with Inertial Measurement Units during Maximal Sprint Acceleration. Sports, 7(9), 202. https://doi.org/10.3390/sports7090202

[31] Cappozzo, A., Catani, F., Della Croce, U., Leardini, A. (1995a). Position and orientation in space of bones during movement: anatomical frame definition and determination. Clinical Biomechanics, 10(4), 171–178. https://doi.org/10.1016/0268-0033(95)91394-t

[32] Wu, G., Siegler, S., Allard, P., Kirtley, C., Leardini, A., Rosenbaum, D., … Stokes, I. (2002). ISB recommendation on definitions of joint coordinate system of various joints for the reporting of human joint motion—part I: ankle, hip, and spine. Journal of Biomechanics, 35(4), 543–548. https://doi.org/10.1016/s0021-9290(01)00222-6

[33] Hol, J. (2011). Sensor Fusion and Calibration of Inertial Sensors, Vision, Ultra-wideband and GPS. Amsterdam, Nederland: Amsterdam University Press.

[34] Roetenberg, D., Luinge, H., Slycke, P. (2009). Xsens MVN: Full 6DOF human motion tracking using miniature inertial sensors. Xsens Motion Technol. BV Tech. Rep.. 3.

[35] Houck, J., Yack, H. J., Cuddeford, T. (2004). Validity and comparisons of tibiofemoral orientations and displacement using a femoral tracking

device during early to mid stance of walking. Gait Posture, 19(1), 76–84. https://doi.org/10.1016/s0966-6362(03)00033-x

[36] Cavallo, A., Cirillo, A., Cirillo, P., De Maria, G., Falco, P., Natale, C., Pirozzi, S. (2014). Experimental Comparison of Sensor Fusion Algorithms for Attitude Estimation, IFAC Proceedings Volumes, Volume 47, Issue 3, 2014, Pages 7585-7591, ISSN 1474-6670, ISBN 9783902823625, https://doi.org/10.3182/20140824-6-ZA-1003.01173.

APPENDIX I

Fig. 13 shows the mean RMSD and STD caused by the STA for all trails of a typical subject. Fig. 14 shows the mean RMSD and STD of the error caused by the orientation filter for all trials of a typical subject.

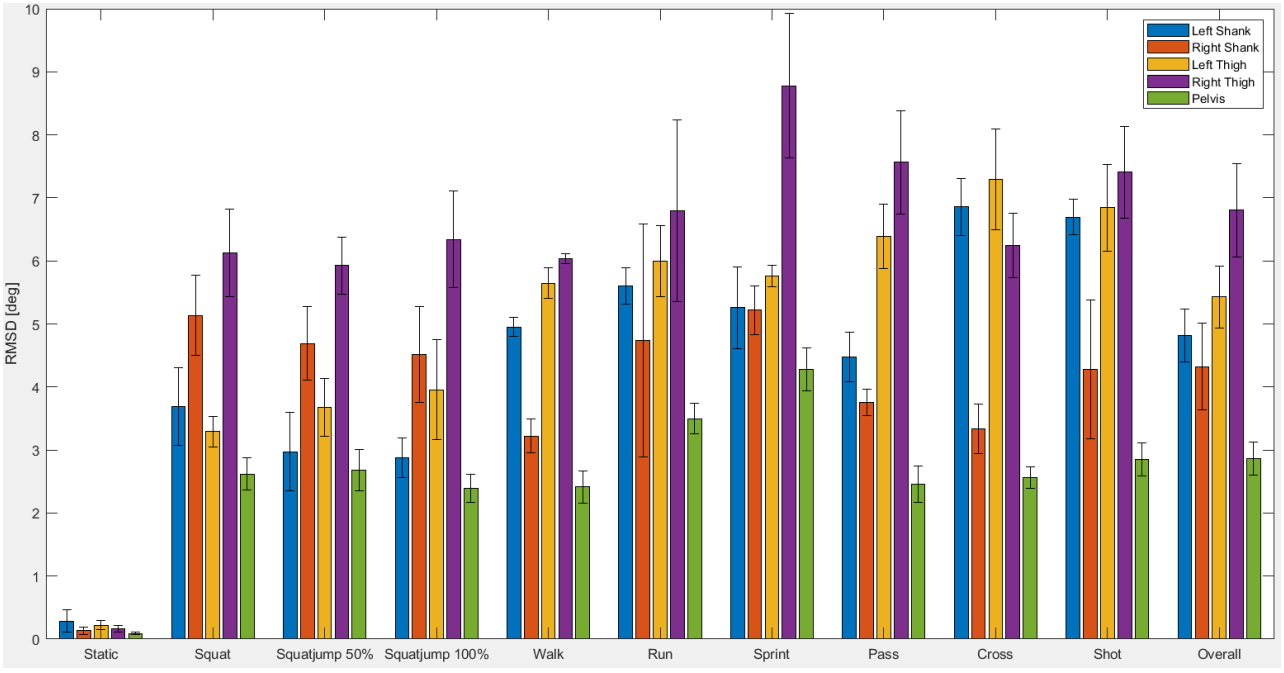

Fig. 13: Error caused by the STA of a typical subject. Mean RMSD and STD for all body segments and all trials

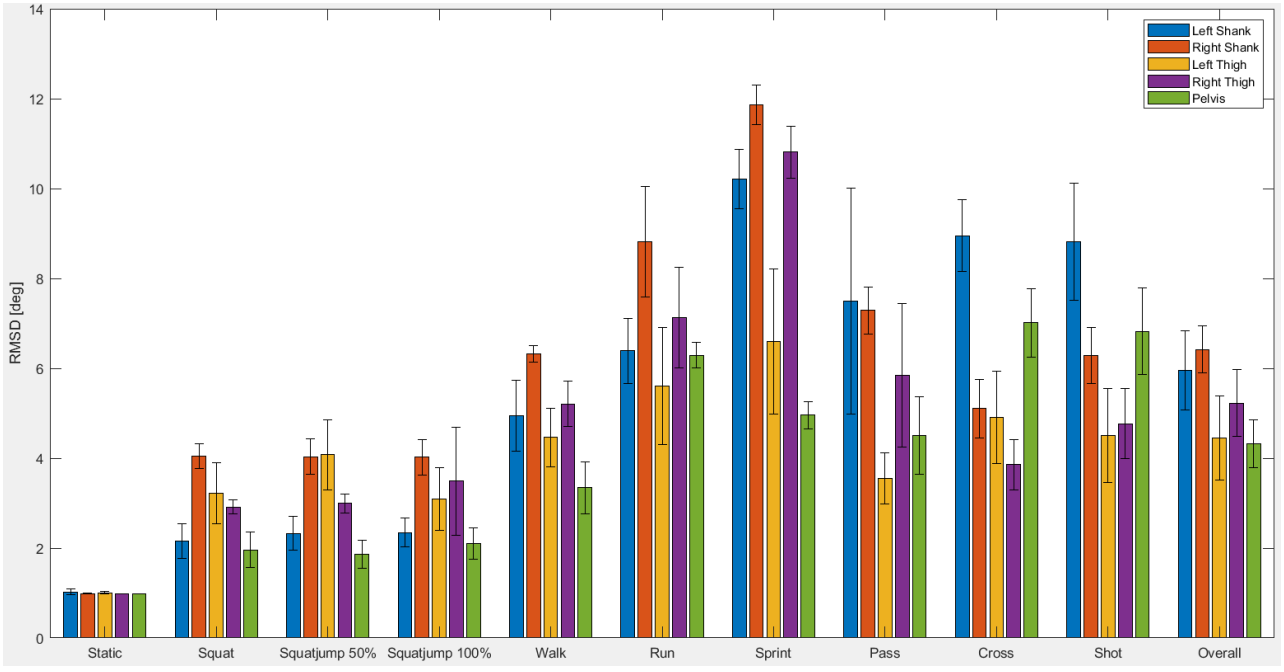

Fig. 14: Error caused by the orientation filter of a typical subject. Mean RMSD and STD for all body segments and all trials

APPENDIX II

Quantification of Error Sources with Inertia Measurement Units in Sports

Haye Kamstra[1,co], *Erik Wilmes*[2,3,co], *Frans van der Helm*[1]

1 Biomechanical Engineering, Faculty of Mechanical, Maritime and Materials Engineering, Delft University of Technology, Delft, the Netherlands

2 Amsterdam Movement Sciences, Department of Human Movement Sciences, Faculty of Behavioural and Movement Sciences, Vrije Universiteit Amsterdam, Amsterdam, The Netherlands

3 FIFA Medical Centre of Excellence, Royal Netherlands Football Association, Zeist, The Netherlands

co Both authors contributed equally to this work

***Abstract*— Inertial measurement units (IMUs) offer the possibility to capture the lower body motions of players of outdoor team sports. However, various sources of error are present when using IMUs: the definition of the body frames, the soft tissue artefact (STA) and the orientation filter. Methods to minimize these errors are currently being used without knowing their exact influence on the various sources of errors. The goal of this study was to present a method to quantify each of the sources of error of an IMU separately. The method was demonstrated for the example of football-specific movements. An optoelectronic system was used as a golden standard. Rigid marker clusters (RMCs) were designed to construct a rigid connection between the IMU and four markers. This allowed for the separate quantification of each of the sources of error. Ten subjects performed nine different trials, varying both in type of movement and in movement intensity. The error of the definition of the body frames (11.3-18.7 deg RMSD), the STA (3.8-9.1 deg RMSD) and the error of the orientation filter (3.0- 12.7 deg RMSD) were all quantified separately. This study is the first study to quantify each of these sources separately and allows future studies to quantify and optimize the effects of error reduction techniques.**

Keywords: inertial measurement unit; soft tissue artefact; orientation filter; error quantification

INTRODUCTION

Human motion analyses can provide valuable information regarding athletic performance in sports. Currently the gold standard for human motion analysis are optoelectronic systems (Ancillao, 2017), which use multiple cameras and skin placed markers on bony anatomical landmarks to capture the motion of the human body. However, this method has some important limitations, including a restricted measurement volume, extensive set-up procedures, high costs, difficulty measuring multiple persons at the same time, and the requirement of expert knowledge. These limitations restrict the use of optoelectronic-based motion analysis to research settings.

The use of inertial measurement units (IMUs) overcomes these issues and allow for human motion analysis outside laboratory settings (Lopez-Nava et al., 2016). An IMU consists of a combination of accelerometers, gyroscopes, and optionally magnetometers. These measurements are combined in a process called 'sensor fusion' to obtain the orientation of the IMU. Therefeore, when IMUs are fixated to body segments, their orientation in space can be estimated. Consequently, recent years have seen an increased interest in IMUs in sports specific settings.

Multiple studies have validated IMUs with optoelectronics for whole body kinematics (Robert-Lachaine et al., 2016), lower body kinematics during gait (Peruzzi et al. 2011, Leardini et al., 2014), lower body kinematics during dynamic movements (Wilmes et al., 2020, Teufl et al., 2019) and upper body kinematics (Morrow et al., 2017, Bergamini et al., 2013). Relative joint angle errors between both methods were present in all studies and ranged from 2 to 14 deg root-mean-square error (RMSE). With IMU-based motion analysis, joint angles are determined by calculating the relative orientation between IMUs on adjacent body segments. Therefore, errors in the orientation estimation of both body segments are propagated to the joint angle errors. To the best of our knowledge, no study has quantified the errors of body segment orientations separately. Moreover, no study has separated these errors to the different sources of error that exist. There are three important sources of error to consider: the definition of the body frames, the soft tissue artefact (STA) and the orientation filter.

Body frames are defined directly from 3D marker positions when using optoelectronics. IMUs however, have their own local coordinate frame attached to the sensor, necessitating a sensor-body calibration procedure to define body frames. These procedures incorporate pre-defined postures (Morton et al., 2013, Palermo et al., 2014, Teufl et al., 2018) or movements (Favre et al., 2009, de Vries et al., 2010), which must be executed by the person being measured. This means that the accuracy of the sensor-body calibration depends on the execution of the calibration movements or postures. Consequently, the definitions of the body frames may differ between optoelectronics and IMU-based motion analysis methods.

The Soft Tissue Artefact (STA) is defined as the error caused by the relative motion between the bone and the skin. STA is the biggest source of error in the field of human motion analysis (Peters et al., 2010). Both optoelectronics and IMUs suffer from STA. However, optoelectronic systems are less vulnerable to STA because it measures marker positions. Markers are relatively far apart, and marker locations are chosen such that relative motion between the markers and bone is minimized. Therefore, the effects on the modeled body segment orientations may be relatively small. An IMU on the other hand, is directly affected by a change in orientation of the skin with respect

to the bone. Especially in sports this may be a problem because of muscles bulging when contracting, and around moments of impact with the ground. However, since STA quantification is difficult and has so far been limited to small scale, low activity studies (Cereatti et al., 2017), no studies have quantified the STA of IMUs.

To estimate the orientation of an IMU, the measurements of the rate gyroscopes are integrated. However, due to integration drift, the computed orientation would suffer from large errors within seconds. To compensate for this drift, both the accelerometers and magnetometers are assumed to measure a constant vector, gravity, and the earths' magnetic field respectively. An orientation filter combines orientation estimates based on these vectors with the rate gyroscope measurements to estimate an IMUs' orientation (Madgwick et al., 2011). In case of magnetic field distortions or linear accelerations the assumption of a constant vectors no longer holds true, which leads to orientation errors (de Vries et al., 2009). To the best of our knowledge, no study has been performed separating the error of IMU-based body segment orientations in the definition of the body frames, the STA and the orientation filter. Consequently, methods to minimize the various errors are currently being used without knowing their exact influence.Therefore, the goal of this study is to present a method to quantify the sources of body segment orientation errors in human motion analysis with IMUs. The errors are quantified for the example of football movements, which we think would be representative for other field sports as well. In addition, various calibration techniques, movement types, and movement intensities are compared to examine their influence on the sources of error. The quantification of these errors can provide a necessary insight for all human motion analysis studies using IMUs and would allow for the optimization of error reduction techniques. In addition, raw data and accompanying software to quantify the different sources of error are openly available to allow other researchers to optimize their own data processing methods and to quantify the performance of different data processing methods. It was hypothesized that different calibration movements, movement intensities, movement types, and different body segments would influence the different sources of error of human motion analysis with IMUs.

METHOD

Subjects and Instrumentation

Ten male subjects (mean $\pm$ std: age [y] 22.6 $\pm$2.2, height [cm] 180.6 $\pm$8.7, weight [kg] 70.3 $\pm$9.8) participated in the study. All subjects were active football players with at least five years experience and had their right leg as their preferred leg of shooting. All subjects signed an informed consent in accordance with the Declaration of Helsinki and the study was approved by the ethics committee of the VU Amsterdam. No subjects had any injury at the time of testing. Subjects were equipped with five IMUs (MPU-9150,Invensense, SanJose, CA, USA). The IMUs were placed on the left and right thigh, left and right shank and on the pelvis, see Fig. 1. Data was gathered at 500 Hz and logged on a SD card inside the IMU, allowing for offline analysis.

Sixteen retro-reflective markers were placed on the following anatomical landmarks: the anterior and posterior superior iliac spines, the posterior side of the thighs halfway the length hip to knee, the medial and lateral femoral epicondyles, the anterior side of each shank halfway the length knee to ankle and the medial and lateral malleoli, see Fig. 1. The location of the markers was captured at 250 Hz with cameras of the Vicon Optoelectronic system (Eight Vicon V5 cameras, Vicon Motion Systems Ltd., Oxford, UK).

A Rigid Marker Cluster (RMC) is a rigid connection between 4 markers and the IMU (Teufl et al., 2019). A 3D model was designed in SolidWorks (SolidWorks 2015, Dassault Systèmes, Winchester, Massachusetts, USA) and printed in PLA with an Ultimaker 3D printer, weighing 41 grams including IMU, see Fig. 1. The position of these markers was also captured at 250 HZ with the Vicon Optoelectronic system. The local coordinate system of the RMCs was defined so that when an IMU was placed inside the RMC, their coordinate systems were aligned.

Protocol

The IMUs were turned on and time synchronized with a mechanical peak in the accelerometers (de Ruiter et al., 2019). The IMUs and markers were fixed to the RMCs with double sided adhesive tape. The RMCs and markers were placed on shaved skin with double sided adhesive tape, see Fig. 1.

A sensor-body calibration was necessary to construct coordinate systems for each body segment. Three different sensor-body calibrations were performed. All calibration methods had the same first step, a static calibration in the neutral pose. In this position the longitudinal axis of each body segment was assumed to be parallel to gravity and could therefore be defined. The second step of the sensor-body calibration was a movement performed in the saggital plane and could therefore be used to define the frontal axis of the body segments. The third axis of the coordinate systems of the body segments was defined orthogonal to the longitudinal and horizontal axis (Wilmes et al., 2020). The three different sensor-calibration movements were: bow and thigh rise(A), squat(B) and inclined plank(C) (Teufl et al., 2018), see Fig. 2. For the inclined plank movement, the subject had to place his hands on an object in front him and move towards this object while keeping his legs and torso in a straight line.

After the sensor-body calibrations, three types of movement were executed at three intensities. The nine trials were: a squat, a squat jump at 50% intensity, a squat jump

Fig. 1: Subject instrumentation. IMUs were placed in the Rigid Marker Clusters and placed on the left and right thigh, left and right shank and pelvis, yellow circles in the figure. Markers were placed on the following anatomical landmarks: the anterior and posterior superior iliac spines, the posterior side of the thighs halfway the length hip to knee, the medial and lateral femoral epicondyles, theanterior side of each shank halfway the length knee to ankle and the medial and lateral malleoli, blue circles in the figure.

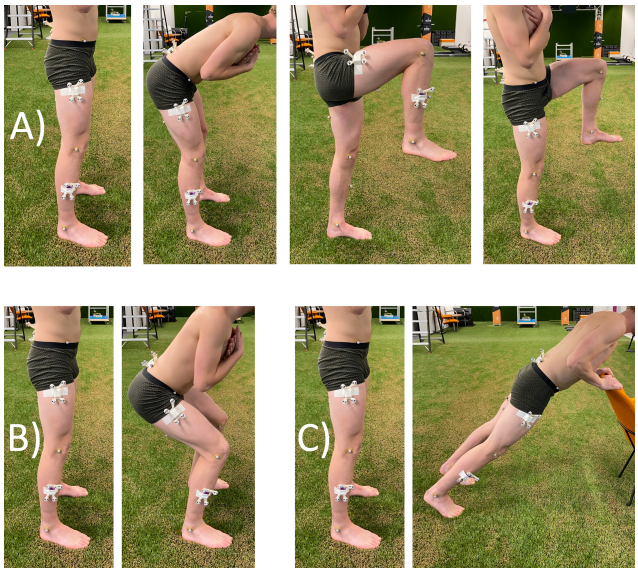

Fig. 2: Sensor-body calibration movements. Calibration A consists of a neutral pose followed by a bow, right thigh rise and left thigh rise. Calibration B consists of a neutral pose and a squat movement. Calibration C consists of a neutral pose and an inclined plank movement.

at 100% intensity, a walk, a run at 50% intensity, a sprint at 100% intensity, a pass, a cross and a shot, all with the right leg. Each trial was repeated eight times.

Data Processing

The raw marker position data was processed in Vicon Nexus (version 2.7.3, Vicon Motion Systems Ltd., Oxford, UK). Possible gaps in marker trajectories were filled using Nexus' Woltring gap fill algorithm, the rigid body gap fill and the kinematic gap fill for gaps of a maximum of 0.05, 0.1 and 0.7 seconds, respectively, according to the recommendations by Visual 3D (C-Motion, Inc, Germantown, MD, USA). Of the eight recorded trials, the first five trials without gaps larger than 0.7 seconds were used for further processing. Marker data was exported to Matlab (version 2020a, The MathWorks, Inc., Natick, MA, USA). A low-pass, fourth order Butterworth filter with a cut-off frequency of 8 Hz was applied to all marker trajectories, based on the recommendations by Visual 3D (C-Motion, Inc, Germantown, MD, USA). Based on the markers on the anatomical landmarks, in combination with a measurement of the leg length, body frames were defined for the left and right thigh, left and right shank and the pelvis, based on Cappozzo et al. (1995) and following ISB recommendations (Wu et al., 2002). These body frames were named the Anatomical Landmark marker calibrated body frames (AL-mcbf). The markers on the RMC were used to construct a RMC sensor frame (RMC-sf) which was aligned with the IMU sensor frame (IMU-sf). Both the orientation of the AL-mcbf and the RMC-sf frames were described as rotation quaternions relative to the global reference frame (GRF) of the Vicon system. Rotation quaternions were used since they provide a continuous description of orientation and do not suffer from difficulties, such as gimbal lock.

IMU data were exported to Matlab and downsampled to 250 Hz to match the frequency of the other data sets. Offsets and misalignment in the IMU sensors were compensated for with an IMU-sensor calibration (Tedaldi et al., 2014, Kok et al., 2016). A gradient decent Madgwick algorithm with a filter gain of 0.043 (Madgwick et al., 2011) was used to compute the orientation of the IMU sensor frame (IMU-sf) relative to the IMU-Reference frame (IRF). The already described sensor-body calibration movements were used to compute the IMU-body frames. The sensor-body calibration procedure was based on Wilmes et al. (2020) and followed the ISB recommendations (Wu et al., 2002). Body frames were constructed for each of the different sensor-body calibration movements. These frames were named the IMU sensor calibrated body frames A-C (IMU-scbf(A-C)) based on which calibration movement was used, see equation 1, (${}^{B}_{A}q$ is the rotation quaternion from frame A to frame B, q_t is a time varying rotation quaternion and q is a time invariant rotation quaternion).

$$ {}^{IMU-scbf(A-C)}_{IRF}q_t = {}^{IMU-sf}_{IRF}q_t \otimes {}^{IMU-scbf(A-C)}_{IMU-sf}q \quad (1) $$

To compare the different frames, all frames must be described relative to the same global frame with a hand-eye calibration (Hol 2011). A large compass with markers at both ends was used to determine the quaternion between the IRF and GRF (Madgwick et al., 2011). This quaternion was then used to describe the IMU-sf and the IMU-scbf(A-C) relative to the GRF, see equation 2 and 3.

$$ {}^{IMU-sf}_{GRF}q_t = {}^{IRF}_{GRF}q \otimes {}^{IMU-sf}_{IRF}q_t \quad (2) $$

$$ {}^{IMU-scbf(A-C)}_{GRF}q_t = {}^{IRF}_{GRF}q \otimes {}^{IMU-scbf(A-C)}_{IRF}q_t \quad (3) $$

Furthermore, to quantify the error of the definition of the body frames, the IMU-sf and RMC-sf were rotated to a marker calibrated body frame, based on the static trial, see equation 4-7. An overview of all data processing steps is provided in Fig. 3.

$$ {}^{IMU-sf}_{AL-mcbf}q = \frac{1}{n}\sum_{t=1}^{n}\left(\left({}^{AL-mcbf}_{GRF}q_t \right)^{-1} \otimes {}^{IMU-sf}_{GRF}q_t \right) \quad (4) $$

$$ {}^{IMU-mcbf}_{GRF}q_t = {}^{IMU-sf}_{GRF}q_t \otimes {}^{AL-mcbf}_{IMU-sf}q \quad (5) $$

$$ {}^{RMC-sf}_{AL-mcbf}q = \frac{1}{n}\sum_{t=1}^{n}\left(\left({}^{AL-mcbf}_{GRF}q_t \right)^{-1} \otimes {}^{RMC-sf}_{GRF}q_t \right) \quad (6) $$

$$ {}^{RMC-mcbf}_{GRF}q_t = {}^{RMC-sf}_{GRF}q_t \otimes {}^{RMC-sf}_{AL-mcbf}q \quad (7) $$

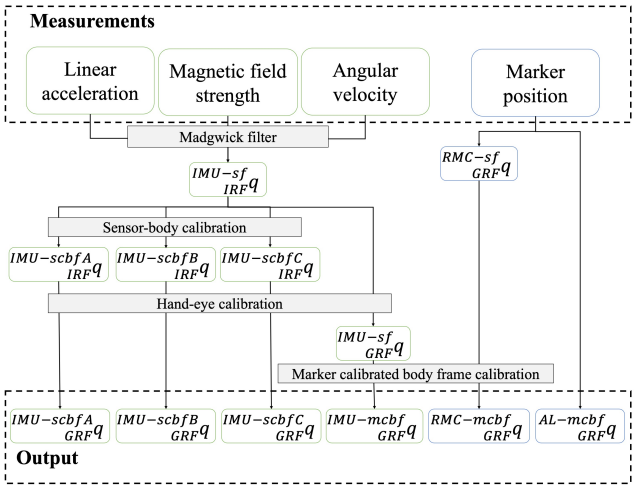

Fig. 3: Flow chart of the data processing. Measurements were converted to rotation quaternions between two frames. IRF = IMU Reference Frame, GRF = Global Reference Frame, IMU-sf = IMU sensor frame, IMU-scbf(A-C) = IMU sensor calibrated body frame A, B and C, RMC-sf = RMC sensor frame, AL-mcbf = Anatomcial Landmarks marker calibrated body frame, IMU-mcbf = IMU marker calibrated body frame and RMC-mcbf = RMC marker calibrated body frame. The sensor-body calibration is based on the different calibration movements(A-C). The hand-eye calibration is based on the marker compass measurement. The marker calibrated body frame calibration is based on a static trial.

TABLE I: Comparisons between the different body frames and the error that the difference in frames describes.

	frame 1	frame 2	Error
#1	IMU-scbfA	IMU-mcbf	Error definition body frames A
#2	IMU-scbfB	IMU-mcbf	Error definition body frames B
#3	IMU-scbfC	IMU-mcbf	Error definition body frames C
#4	RMC-mcbf	AL-mcbf	STA
#5	IMU-mcbf	RMC-mcbf	Error orientation filter
#6	IMU-mcbf	AL-mcbf	Error orientation filter + STA
#7	IMU-scbfA	AL-mcbf	Total error with calibration A
#8	IMU-scbfB	AL-mcbf	Total error with calibration B
#9	IMU-scbfC	AL-mcbf	Total error with calibration C

Data Analysis

After data processing, six different body frames (IMU-scbfA, IMU-scbfB, IMU-scbfC, IMU-mcbf, RMC-mcbf and AL-mcbf) are described relative to the global frame for each body segment. Table 1 shows the comparisons between the frames that were made.

As described in the introduction, there were three main sources of error between IMUs and an optoelectronic system: the definition of the body frames, the soft tissue artefact (STA) and the orientation filter. In comparison 1-3 the same measurements were used to compute the orientation of the body segments. However, since different sensor-body calibration methods were used, the difference in these comparisons is the error caused by the definition

of the body frames. In comparison 4 the frames were constructed from measurements of the optoelectronic system and were therefore not influenced by the orientation filter. In addition, the frames were calibrated to the same body frame. Consequently, comparison 4 entails the relative motion between the body frames obtained using the markers on bony landmarks and the body frames obtained using the rigid marker cluster with a rigid connection to the IMU. This relative motion is caused by the STA. In comparison 5, there was a rigid connection between the IMU and the RMC preventing the influence of STA. And because both frames were aligned, no error from the definition of the body frames was present. Therefore, the error found in comparison 5 was the error caused by the orientation filter. In comparison 6 the orientations obtained from the IMUs were expressed in the same body frame as the orientations obtained from the markers on bony landmarks, ruling out the error of body frame definitions. Therefore, the difference was the combined error of the orientation filter and the STA. In comparison 7-9 the IMU body frames were calibrated based on the calibration movements(A-C). Therefore, the difference in these comparisons included the error caused by the definition of the local frames, the STA and the orientation filter.

Each comparison was described by the rotation quaternion between the two frames. From this quaternion the smallest rotation between the two frames was calculated in degrees. For each trial the root mean square difference (RMSD) of the smallest angle between the frames was calculated. For each subject the mean over five repetitions of all nine different trials was calculated. Subsequently the mean and standard deviation (STD) of the RMSD over all subjects was calculated for each trial and each body segment. A three-way repeated measures ANOVA with Bonferroni post-hoc comparisons were performed to assess the effects of movement type, intensity, and body segment (3 movement types x 3 intensities x 5 segments) on the STA errors, orientation filter errors, the total errors. A Greenhouse-Geisser correction was applied if the assumption of sphericity was not met. The significance level was set at p ¡ 0.05 and effect size was calculated as eta squared(2).

RESULTS

Definition Body Frames

Fig. 4 shows the RMSD and STD of the error of the definition of the body frames for calibration A, B and C. The error of the definition of the body frames was constant over time and thus constant for all trials of each subject. No calibration method significantly outperformed the others. The errors ranged between 11.3 and 18.7 deg RMSD. All three calibration methods showed large between subject variability with a STD of up to 8.8 deg.

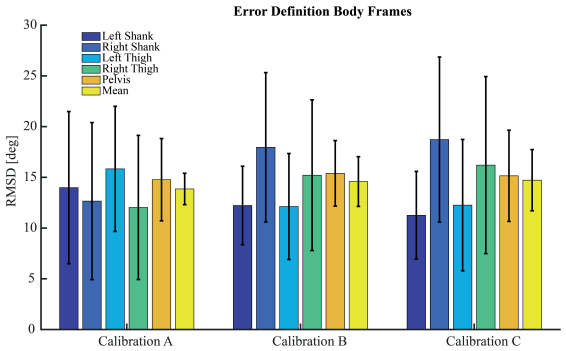

Fig. 4: Error of the definition of the body frames. RMSD of all body segments for the 3 different calibrations, see Fig. 3 for calibration movements.

Soft Tissue Artefact

Table II shows the main and interaction effects on the error caused by the STA. Movement type, intensity and segment were all significant main effects. The results of all Bonferroni post-hoc tests and results of a single subject were included in the Appendix (Fig. 8-13). The RMSD of the STA ranged from 3.8 degrees on the pelvis during the walk trial, to 9.1 degrees on the right thigh during the sprint trial. Fig. 5 shows the error caused by the STA plotted over time for each trial of a random subject. In the top right corner of each plot the mean RMSD overall body segments and the maximum error are displayed in degrees. It can be seen that the STA is not a constant offset or white noise but that the error is very much time dependent. For the squatting trials, the STA arises during the flexion of the knees, both before push-off and after landing for the squatjumps. For the walk, run and sprint trial, the STA shows a cyclic pattern related to the gait cycle. The shooting trials display a spike of the left thigh before ball contact and a spike of the right thigh directly after ball contact. The spike before ball contact is caused by the landing of the stance leg, the spike after ball contact by the ball contact and the swing through of the shooting leg. The maximum error in time occurred during the shot trial on the right thigh and was 34.4 degree.

Orientation filter

Table II shows the main and interaction effects on the error caused by the orientation filter. Movement type, intensity and segment were all significant main effects. The RMSD of the error caused by the orientation filter ranged from 3.0 degrees on the left shank during the squat trial to 12.7 degrees on the left shank during the sprint trial. Fig. 6 shows the error caused by the orientation filter plotted over time for the same subject and the same trials as in Fig. 5. The error caused by the orientation filter is highly time dependent. The error over time consists of a constant offset of around 1 degree, some high frequency behaviour around moments of impact and some low frequency behaviour related to movement. For the squatting

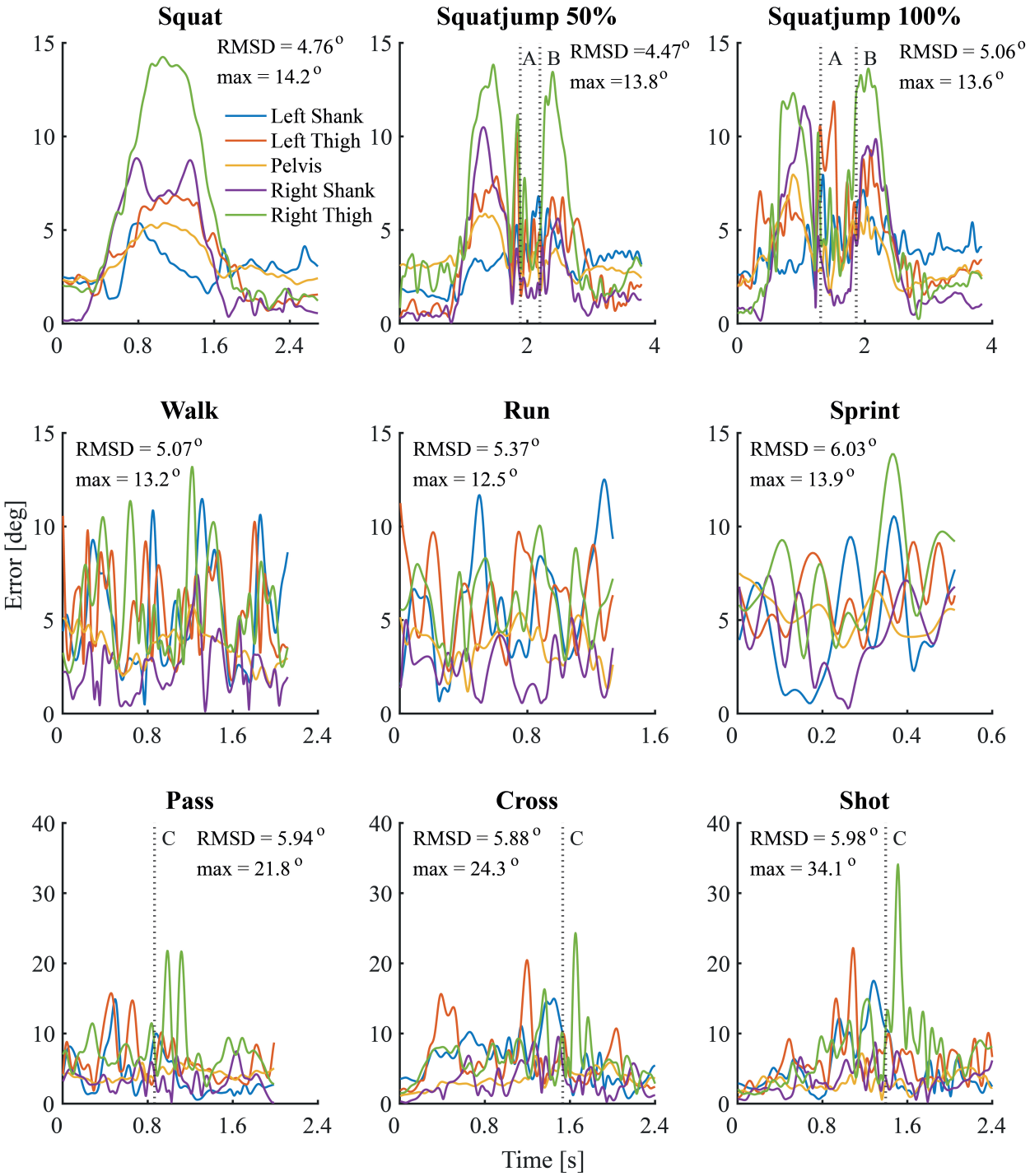

Fig. 5: Error caused by the STA, plotted for each trial over time of a typical subject. In the top right corner of each plot the RMSD overall body segments and maximum error are displayed in degrees. The vertical dashed line represents a specific moment in time: A = push off, B = landing, C = ball contact.

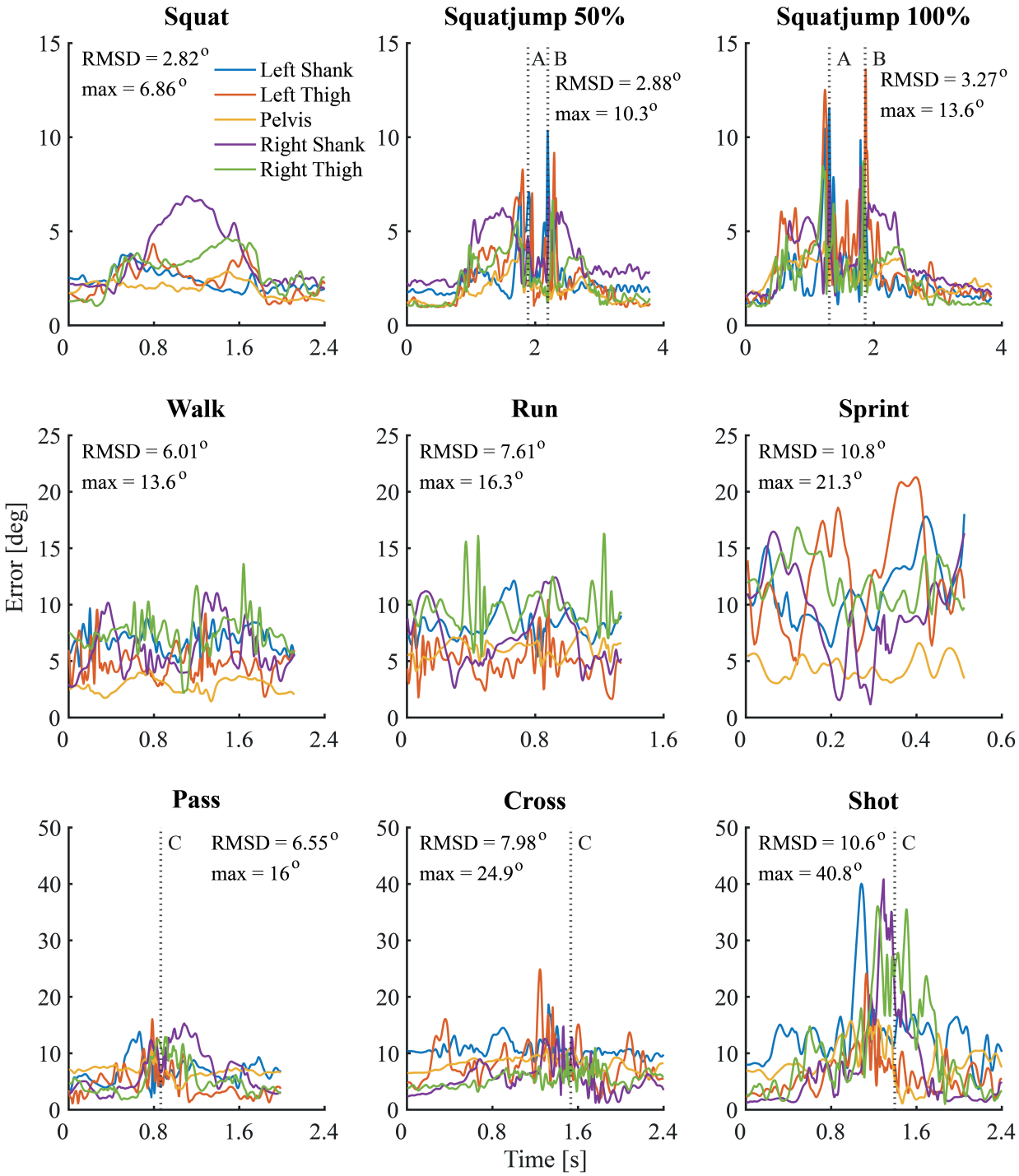

Fig. 6: Error of the orientation filter, plotted for each trial over time of a typical subject. The exact same trails were used in Fig. 5. In the top right corner of each plot the RMSD overall body segments and maximum error are displayed in degrees. The vertical dashed line represents a specific moment in time: A = push off, B = landing, C = ball contact.

TABLE II: Significance and effect size of main and interaction effect of movement type, intensity and segment on the RMSD of the error caused by the STA, the Orientation Filter and the Total Error. Insignificant effects were denoted with an astrix(*)

	Error STA		Error Orientation Filter		Total Error	
	p	η^2	p	η^2	p	η^2
Movement type	<0.001	0.100	<0.001	0.201	<0.001	0.046
Intensity	<0.001	0.052	<0.001	0.066	<0.001	0.008
Segment	<0.001	0.154	0.018	0.104	0.604*	0.040
Movement type : Intensity	<0.001	0.042	<0.001	0.063	0.046	0.003
Movement type : Segment	<0.001	0.132	0.006	0.055	<0.001	0.038
Intensity : Segment	0.750*	0.004	<0.001	0.019	<0.001	0.008
Movement type : Intensity : Segment	0.001	0.025	0.003	0.012	<0.001	0.009

trials, the error of the orientation filter arises during the flexion of the knees, both before push-off and after landing for the squatjumps. For the walk, run and sprint trial, the error of the orientation filter shows a cyclic pattern related to the gait cycle. The shooting trials display high frequency behaviour around the moment of ball contact. A relationship between movement intensity and maximum error in time is visible. The maximum error in time occurred during the shot trial on the right shank and was 41.2 degrees.

Total Error

Fig. 7 shows the mean RMSD and STD for each of the sources of error, for the combined error of the STA and the orientation filter and for the total error, averaged over all trials. To reduce the amount of displayed data the error of the definition of the body frames and the total error is only displayed for sensor-body calibration A. The mean RMSD and STD of the combined error of the STA and the orientation filter and of the total error are also shown for each trial in the Appendix.

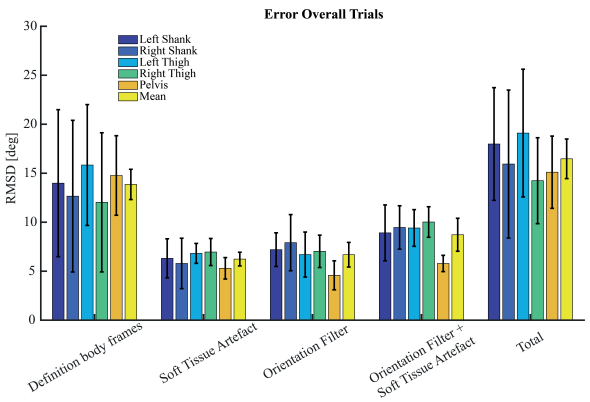

Fig. 7: RMSD and STD for each of the sources of error and total error, for all body segments, mean overall trials. The error of the definition of the body frames and the total error is displayed for calibration A.

DISCUSSION AND IMPLICATIONS

The goal of this study was to present a method to quantify the sources of body segment orientation errors in human motion analysis with IMUs. In addition, the influence of different sensor-body calibration methods, different movements, and movement intensities on the sources of error were studied. The sources of error were quantified by comparing the IMUs against an optoelectronic system. It should be noted that the optoelectronic system is not a golden standard in all cases and therefore the results were described by root-mean-square differences (RMSD) instead of root-mean-square error. Another important notion is that because the goal of this study was to get a complete insight in the different sources of error, no error minimization techniques were used on the IMU data. In current literature this is not the case. Furthermore, unlike current literature, this study described the orientation of body segments instead of joint angles. This choice was also made to get a greater insight in the different sources of error, since joint angle errors comprise the errors of the IMU on the body segment proximal to the joint and the errors of the IMU on the body segment distal to the joint.

Definition Body Frames

The definition of the body frames was the largest source of error for the IMUs. The high between subject variability shows that there are subject specific factors that cause a difference. This difference could arbitrarily be attributed to either the IMUs or the optoelectronic system, depending on which one is chosen as the golden standard. The high between subject variability could be caused by inconsistent execution of the calibration movements, or by inconsistent anthropometry or marker placement, which would influence the marker calibrated body frames.

A study by Robert-Lachaine et al. (2017) also compared the defined body frames of IMUs with an optoelectonic system. The results ranged from 2.5 - 7.0 deg RMSE of the joint Euler angles of the lower extremities. This considerably smaller error could be explained by the fact that this study used the Xsens MVN model. The MVN model uses a combination of static postures, anthropometric measures, and boundary conditions to define body frames (Roetenberg et al., 2009).

The used method in this study was able to quantify the error of the definition of the body frames. The definition of the body frames with IMUs could possibly be improved by using models, like the Xsens MVN model. However, the great advantage of IMUs is their ease of use, easy

placement method and short set-up time. Therefore, there exists a trade-off between accuracy of the definition of the body frames and practicality for each specific application. However, as shown in current study, differences in the method to define body frames can lead to relatively large differences in estimated body segment orientations. A standardized method for body frame definitions using IMUs would allow for better comparison between studies.

Soft Tissue Artefact

Fig. 5 shows that the method of this study was also able to analyse the STA over time. High frequency STA was seen at moments of impact, like the landing of the squat jumps and around the moment of ball contact for the shooting trials. However, especially for the squat trials, the range of motion had a much larger influence on the RMSD of the STA. This part of the STA is caused by skin sliding and is related to the flexion or extension of a joint close to the IMU. This can be seen in Fig. 8 by the high STA of the pelvis during the squat trials, during which there is lower back flexion. In all other trails there is little or none lower back flexion and thus less STA on the pelvis.

A limitation of the current method is that the STA is quantified relative to an optoelectronic system, of which the markers also suffer from STA. Golden standard STA quantification techniques require either the surgical placement of bone pins (Houck et al., 2004) or the use of medical imaging techniques, like fluoroscopy (Gao et al., 2007). However, these techniques are highly unsuitable for dynamic activities. Consequently, there is no available literature regarding STA in dynamic sports activities to compare present results to. Since the markers of the optoelectronic system are placed on bony landmarks, and the IMUs somewhere on the middle of a segment, the relative STA between the two systems was assumed to be a good approximation of the absolute STA of the IMUs. Another limitation of the current method is that the IMUs were placed in the RMCs. This increases the mass of the object fixated on the skin and because part of the STA is caused by inertia, the STA is likely to be overestimated in this study.

To the best of our knowledge, current study is the first study to quantify the STA during dynamic activities and the first study to quantify the STA of IMUs. The used method was able to show the dependence of STA on movement type, movement intensity and body segment. However, the noted limitations should be taken into consideration when interpreting the absolute values of the results. Yet, the low within subject variability (see Appendix, Fig. 12) does indicate good repeatability of the method.

Orientation filter

Although there was high variability in the results, a dependency of the error of the orientation filter on movement type, intensity and segment was shown. However, the within subject variability was much lower (the results of a single subject are displayed in the Appendix, see Fig. 13.). This indicates that the high variability is caused by between subject factors. The main factor is expected to be the use of different IMUs. Although all IMUs were both initialized and calibrated in the same way, a difference in performance was noticed. In Fig. 6 the error caused by the orientation filter could be split up in a constant offset, low frequency behaviour, and high frequency behaviour. The constant offset and the low frequency behaviour could have different causes, including misalignment of the sensors within the IMU, noise in the sensors or distortions in the local magnetic field. Furthermore, despite careful sensor calibration procedures, small biases in the sensor measurements may still have been present or may have reappeared after calibration. The high frequency behaviour is expected to be caused by moments of impact, like landing after a squatjump or around the moment of ball contact. During these moments the body segments undergo substantial accelerations, making the direction of the resultant acceleration measured by the accelerometers no longer aligned with gravity.

A study by Cavallo et al. (2014) used a robotic arm to quantify the error of different orientation filters. For slow rotations (18 deg/s) the Madgwick filter had an error of 5.13 degrees RMSE and 7.07 degrees RMSE for fast rotations (45 deg/s). Since in this study the IMU was only rotated, the influence of linear accelerations was not captured. Furthermore, during the sprint trials angular velocities of up to 1000 deg/s were measured, which are of a far larger magnitude than the study by Cavallo et al. (2014). Another difference with the current study is that a robotic arm was used as golden standard instead of an optoelectronic system. At dynamic moments of impact and high accelerations, there were gaps in the marker data, which were filled using gap fill algorithms. Especially for dynamic movements, the use of these gap fill algorithms, but also the use of low pass filters, could lead to a reduction of the actual peak orientations. However, based on the low within subject variability (see Appendix, Fig. 13) and the agreement in magnitude with previous studies, we are confident that with present method we were be able to quantify the error caused by the orientation filter.

Total Error

The total error captured the combined effect of each of the three individual errors. Also, the combined effect of the STA and the error caused by the orientation filter was quantified. The combined effect was approximately the square root of the square of the individual errors, for both the combined effect of the STA and orientation filter and for the total error. This implies that the individual errors are roughly independent of one another.

A study by Wilmes et al. (2020) validated IMUs with

an optoelectronic system for a range of dynamic football movements. Across all movements, an average error of 5.3 degrees RMSD was reported for knee flexion/extension angles and 8.0 degrees RMSD for hip flexion/extension angles. These lower RMSDs are expected to be caused by the use of filter techniques on the IMU data. In the current study no filtering techniques were used to get insight in the complete error caused by the different sources. Another difference is the use of joint angles instead of segment orientations.

Conclusion and Recommendations

This study showed a method to quantify the different sources of body segment orientation errors of human motion analysis with IMUs. During dynamic football activities, the errors of definition of the body frames ranged 11.3 to 18.7 deg RMSD, the STA errors ranged 3.8 to 9.1 deg RMSD, and the error caused by the orientation filter ranged 3.0 to 12.7 deg RMSD. Type of movement, movement intensity and body segment were found to have a significant effect on the errors. Future studies should take these errors into account since they influence IMU-based human motion analysis. In addition, this study highlights the importance of standardizing the methods to define body frames with IMUs. Furthermore, both raw data and data processing scripts of the current study were openly published to give other researchers the opportunity to optimize their own data processing methods and to quantify the performance of different data processing methods.

Data Availability

The data and Matlab scripts for the data processing steps that support the findings of this study are openly available in Zenedo at http://doi.org/10.5281/zenodo.6610795.

Declaration of Competing Interest

The authors have no conflict of interest related to this study.

Acknowledgements

The authors would like to thankfully acknowledge the Dutch Royal Football Association (KNVB) for facilitating the research programme by giving access to their research facilities. This study is part of the research programme "Citius Altius Sanius" with project number P16-28 project 6, which is (partly) financed by the Dutch Research Council (NWO).

References

1. Ancillao, A. (2017). Stereophotogrammetry in Functional Evaluation: History and Modern Protocols. Modern Functional Evaluation Methods for Muscle Strength and Gait Analysis, 1–29. https://doi.org/10.1007/978-3-319-67437-7-1

2. Andersen, M. S., Damsgaard, M., Rasmussen, J., Ramsey, D. K., Benoit, D. L. (2012). A linear soft tissue artefact model for human movement analysis: Proof of concept using in vivo data. Gait Posture, 35(4), 606–611. https://doi.org/10.1016/j.gaitpost.2011.11.032

3. Bergamini, E., Guillon, P., Camomilla, V., Pillet, H., Skalli, W., Cappozzo, A. (2013). Trunk Inclination Estimate During the Sprint Start Using an Inertial Measurement Unit: A Validation Study. Journal of Applied Biomechanics, 29(5), 622–627. https://doi.org/10.1123/jab.29.5.622

4. Cappello, A., Stagni, R., Fantozzi, S., Leardini, A. (2005). Soft Tissue Artifact Compensation in Knee Kinematics by Double Anatomical Landmark Calibration: Performance of a Novel Method During Selected Motor Tasks. IEEE Transactions on Biomedical Engineering, 52(6), 992–998. https://doi.org/10.1109/tbme.2005.846728

5. Cappozzo, A., Catani, F., Della Croce, U., Leardini, A. (1995a). Position and orientation in space of bones during movement: anatomical frame definition and determination. Clinical Biomechanics, 10(4), 171–178. https://doi.org/10.1016/0268-0033(95)91394-t

6. Cavallo, A., Cirillo, A., Cirillo, P. De Maria, G. Falco, P. Natale, C. Pirozzi, S. (2014) Experimental Comparison of Sensor Fusion Algorithms for Attitude

Estimation, IFAC Proceedings Volumes, 47(3), 7585-7591, https://doi.org/10.3182/20140824-6-ZA-1003.01173.

7. Cereatti, A., Bonci, T., Akbarshahi, M., Aminian, K., Barré, A., Begon, M., ... Camomilla, V. (2017). Standardization proposal of soft tissue artefact description for data sharing in human motion measurements. Journal of Biomechanics, 62, 5–13. https://doi.org/10.1016/j.jbiomech.2017.02.004

8. Favre, J., Aissaoui, R., Jolles, B. M., de Guise, J. A., Aminian, K. (2009). Functional calibration procedure for 3D knee joint angle description using inertial sensors. Journal of Biomechanics, 42(14), 2330–2335. https://doi.org/10.1016/j.jbiomech.2009.06.025

9. Gao, B., Conrad, B., Zheng, N. (2007). Comparison of Skin Error Reduction Techniques for Skeletal Motion Analysis. Journal of Biomechanics, 40, S551. https://doi.org/10.1016/s0021-9290(07)70541-9

10. Garling, E. H., Kaptein, B. L., Mertens, B., Barendregt, W., Veeger, H. E. J., Nelissen, R. G. H. H., Valstar, E. R. (2007). Soft-tissue artefact assessment during step-up using fluoroscopy and skin-mounted markers. Journal of Biomechanics, 40, S18–S24. https://doi.org/10.1016/j.jbiomech.2007.03.003

11. Hol, J. (2011). Sensor Fusion and Calibration of Inertial Sensors, Vision, Ultra-wideband and GPS. Amsterdam, Nederland: Amsterdam University Press.

12. Houck, J., Yack, H. J., Cuddeford, T. (2004). Validity and comparisons of tibiofemoral orientations and displacement using a femoral tracking device during early to mid stance of walking. Gait Posture, 19(1), 76–84. https://doi.org/10.1016/s0966-6362(03)00033-x

13. Kok, M., Schon, T. B. (2016). Magnetometer Calibration Using Inertial Sensors. IEEE Sensors Journal, 16(14), 5679–5689. https://doi.org/10.1109/jsen.2016.2569160

14. Kuo, M.-Y., Tsai, T.-Y., Lin, C.-C., Lu, T.-W., Hsu, H.-C., Shen, W.-C. (2011). Influence of soft tissue artifacts on

the calculated kinematics and kinetics of total knee replacements during sit-to-stand. Gait Posture, 33(3), 379–384. https://doi.org/10.1016/j.gaitpost.2010.12.007

15. Leardini, A., Lullini, G., Giannini, S., Berti, L., Ortolani, M., Caravaggi, P. (2014). Validation of the angular measurements of a new inertial-measurement-unit based rehabilitation system: comparison with state-of-the-art gait analysis. Journal of NeuroEngineering and Rehabilitation, 11(1), 136. https://doi.org/10.1186/1743-0003-11-136

16. Lopez-Nava, I. H., Munoz-Melendez, A. (2016). Wearable Inertial Sensors for Human Motion Analysis: A Review. IEEE Sensors Journal, 16(22), 7821–7834. https://doi.org/10.1109/jsen.2016.2609392

17. Ludwig, S.A., Burnham, K.D., Jiménez, A.R., Touma, P.A. (2018). Comparison of attitude and heading reference systems using foot mounted MIMU sensor data: basic, Madgwick, and Mahony. Proc. SPIE 10598, Sensors and Smart Structures Technologies for Civil, Mechanical, and Aerospace Systems 2018, 105982L (27 March 2018); https://doi-org.tudelft.idm.oclc.org/10.1117/12.2296568

18. Madgwick, S. O. H., Harrison, A. J. L., Vaidyanathan, R. (2011). Estimation of IMU and MARG orientation using a gradient descent algorithm. 2011 IEEE International Conference on Rehabilitation Robotics, 1–32. https://doi.org/10.1109/icorr.2011.5975346

19. Morrow, M. B., Lowndes, B., Fortune, E., Kaufman, K. R., Hallbeck, M. S. (2017). Validation of Inertial Measurement Units for Upper Body Kinematics. Journal of Applied Biomechanics, 33(3), 227–232. https://doi.org/10.1123/jab.2016-0120

20. Morton, L., Baillie, L., Ramirez-Iniguez, R. (2013) "Pose calibrations for inertial sensors in rehabilitation applications," 2013 IEEE 9th International Conference on Wireless and Mobile Computing, Networking and Communications (WiMob), Lyon, 2013, pp. 204-211, doi: 10.1109/WiMOB.2013.6673362.

21. Palermo, E., Rossi, S., Marini, F., Patanè, F., Cappa, P. (2014). Experimental evaluation of accuracy and repeatability of a novel body-to-sensor calibration procedure for inertial sensor-based gait analysis. Measurement, 52, 145–155. https://doi.org/10.1016/j.measurement.2014.03.004

22. Peruzzi, A., Della Croce, U., Cereatti, A. (2011). Estimation of stride length in level walking using an inertial measurement unit attached to the foot: A validation of the zero velocity assumption during stance. Journal of Biomechanics, 44(10), 1991–1994. https://doi.org/10.1016/j.jbiomech.2011.04.035

23. Peters, A., Galna, B., Sangeux, M., Morris, M., Baker, R. (2010). Quantification of soft tissue artifact in lower limb human motion analysis: A systematic review. Gait Posture, 31(1), 1–8. https://doi.org/10.1016/j.gaitpost.2009.09.004

24. Robert-Lachaine, X., Mecheri, H., Larue, C., Plamondon, A. (2016). Validation of inertial measurement units with an optoelectronic system for whole-body motion analysis. Medical Biological Engineering Computing, 55(4), 609–619. https://doi.org/10.1007/s11517-016-1537-2

25. Robert-Lachaine, X., Mecheri, H., Larue, C., Plamondon, A. (2017). Accuracy and repeatability of single-pose calibration of inertial measurement units for whole-body motion analysis. Gait Posture, 54, 80–86. https://doi.org/10.1016/j.gaitpost.2017.02.029

26. Robert-Lachaine, X., Mecheri, H., Larue, C., Plamondon, A. (2017b). Effect of local magnetic field disturbances on inertial measurement units accuracy. Applied Ergonomics, 63, 123–132. https://doi.org/10.1016/j.apergo.2017.04.011

27. Roetenberg, Daniel Luinge, Henk Slycke, Per. (2009). Xsens MVN: Full 6DOF human motion tracking using miniature inertial sensors. Xsens Motion Technol. BV Tech. Rep.. 3.

28. Rouhandeh, A., Joslin, C., Zhen Qu, Yuu Ono. (2014). Non-invasive assessment of soft-tissue artefacts in hip joint kinematics using motion capture data and ultrasound depth measurements. 2014 36th Annual International Conference of the IEEE Engineering in Medicine and Biology Society, 1–2. https://doi.org/10.1109/embc.2014.6944585

29. de Ruiter, C. J., van Dieën, J. H. (2019). Stride and Step Length Obtained with Inertial Measurement Units during Maximal Sprint Acceleration. Sports, 7(9), 202. https://doi.org/10.3390/sports7090202

30. Tedaldi, D., Pretto, A., Menegatti, E. (2014). A robust and easy to implement method for IMU calibration without external equipments. 2014 IEEE International Conference on Robotics and Automation (ICRA), 3042–3049. https://doi.org/10.1109/icra.2014.6907297

31. Teufl, W., Lorenz, M., Miezal, M., Taetz, B., Fröhlich, M., Bleser, G. (2018). Towards Inertial Sensor Based Mobile Gait Analysis: Event-Detection and Spatio-Temporal Parameters. Sensors, 19(1), 38–58. https://doi.org/10.3390/s19010038

32. Teufl, W., Miezal, M., Taetz, B., Fröhlich, M., Bleser, G. (2019). Validity of inertial sensor based 3D joint kinematics of static and dynamic sport and physiotherapy specific movements. PLOS ONE, 14(2), e0213064. https://doi.org/10.1371/journal.pone.0213064

33. de Vries, W. H. K., Veeger, H. E. J., Baten, C. T. M., van der Helm, F. C. T. (2009). Magnetic distortion in motion labs, implications for validating inertial magnetic sensors. Gait Posture, 29(4), 535–541. https://doi.org/10.1016/j.gaitpost.2008.12.004

34. de Vries, W. H. K., Veeger, H. E. J., Cutti, A. G., Baten, C., van der Helm, F. C. T. (2010). Functionally interpretable local coordinate systems for the upper extremity using inertial magnetic measurement systems. Journal of Biomechanics, 43(10), 1983–1988. https://doi.org/10.1016/j.jbiomech.2010.03.007

35. Wilmes, E., de Ruiter, C. J., Bastiaansen, B. J. C., Zon, J. F. J. A. van, Vegter, R. J. K., Brink, M. S., … Savelsbergh, G. J. P. (2020). Inertial Sensor-Based Motion Tracking in Football with Movement Intensity Quantification. Sensors, 20(9), 2527. https://doi.org/10.3390/s20092527

36. Wu, G., Siegler, S., Allard, P., Kirtley, C., Leardini, A., Rosenbaum, D., … Stokes, I. (2002). ISB recommendation on definitions of joint coordinate system of various joints for the reporting of human joint motion—part I: ankle,

hip, and spine. Journal of Biomechanics, 35(4), 543–548. https://doi.org/10.1016/s0021-9290(01)00222-6

APPENDIX III

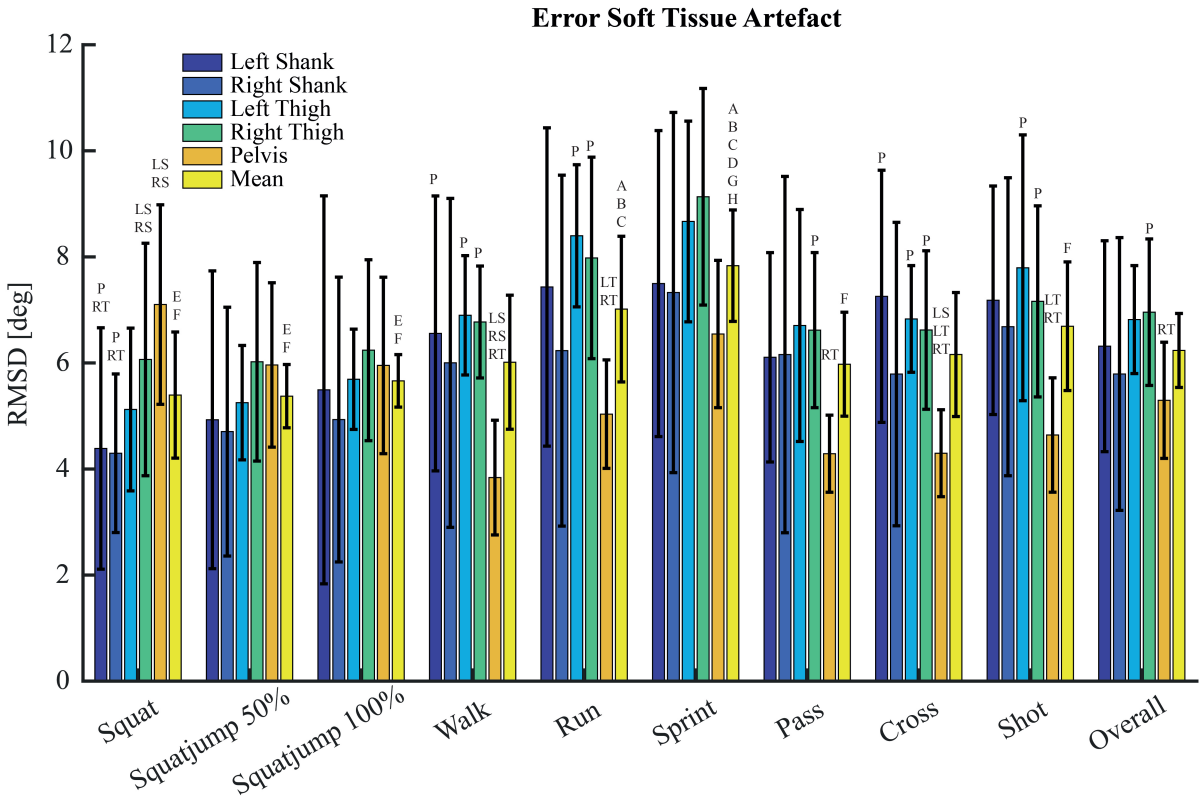

Fig. 8: Error caused by the STA. Mean RMSD and STD for all body segments and all trials. Significant differences within each trial between body segments are displayed by letters above the bar, LS, RS, LT, RT, and P mean a significant difference with the left shank, right shank, left thigh, right thigh, and pelvis, respectively. Significant differences between trails are display with a letter above the mean bar. A = squat, B = squatjump 50%, C = squatjump 100%, D = walk, E = run, F = sprint, G = pass, H = cross and I = shot.

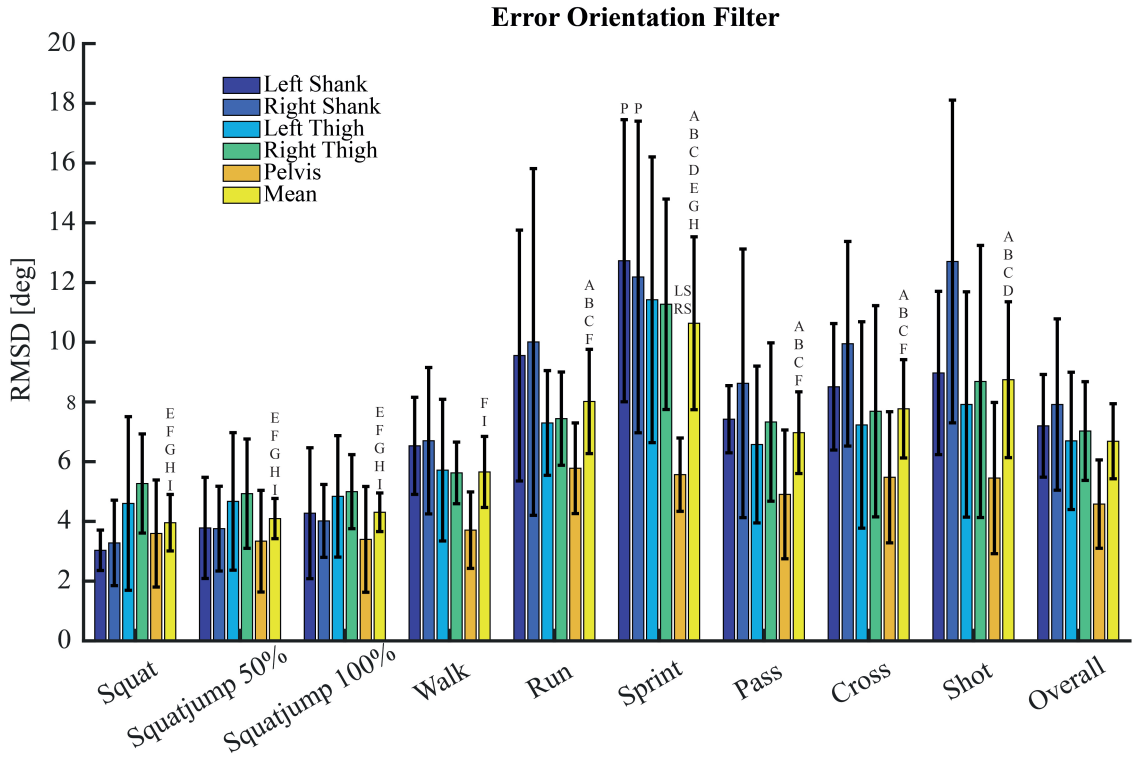

Fig. 9: Error of the orientation filter. Mean RMSD and STD for all body segments and all trials. Significant differences within each trial between body segments are displayed by letters above the bar, LS, RS, LT, RT, and P mean a significant difference with the left shank, right shank, left thigh, right thigh and pelvis, respectively. Significant differences between trails are display with a letter above the mean bar. A = squat, B = squatjump 50%, C = squatjump 100%, D = walk, E = run, F = sprint, G = pass, H = cross and I = shot.

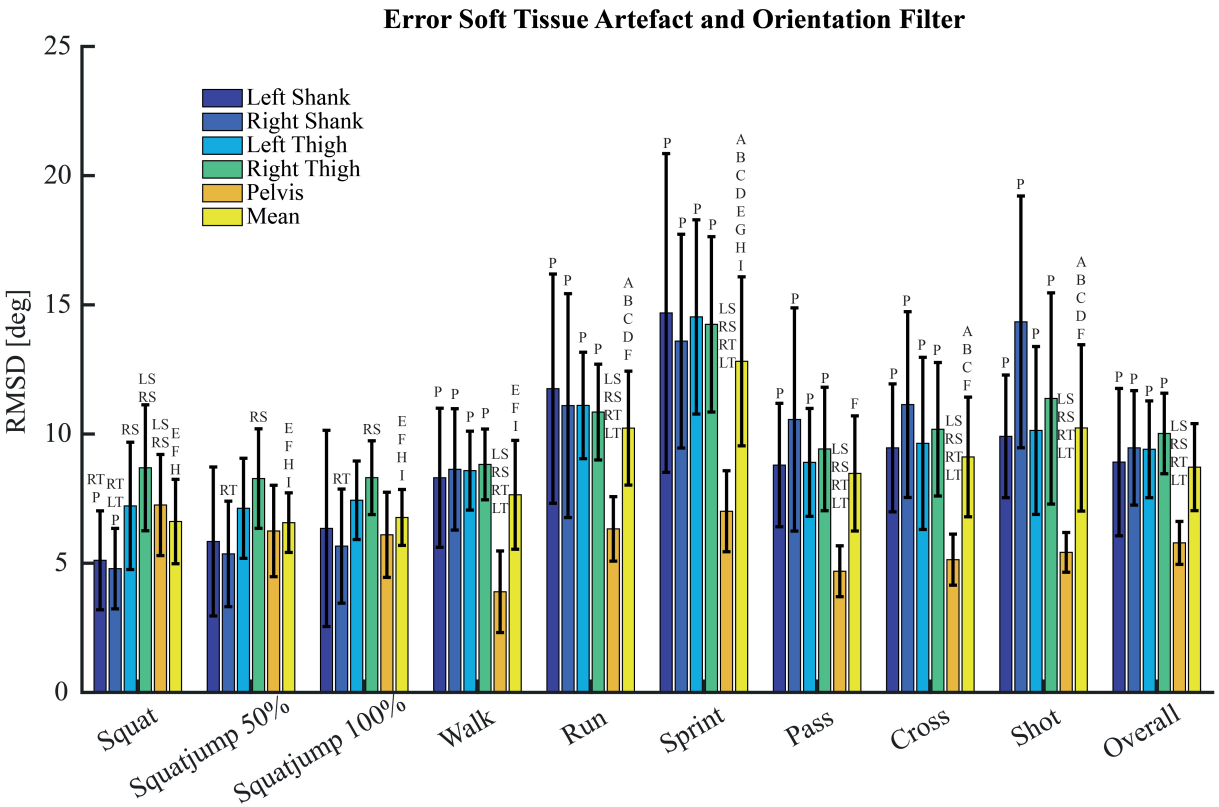

Fig. 10: Combined error of the STA and the orientation filter. Mean RMSD and STD for all body segments and all trials. Significant differences within each trial between body segments are displayed by letters above the bar, LS, RS, LT, RT, and P mean a significant difference with the left shank, right shank, left thigh, right thigh, and pelvis, respectively. Significant differences between trails are display with a letter above the mean bar. A = squat, B = squatjump 50%, C = squatjump 100%, D = walk, E = run, F = sprint, G = pass, H = cross and I = shot.

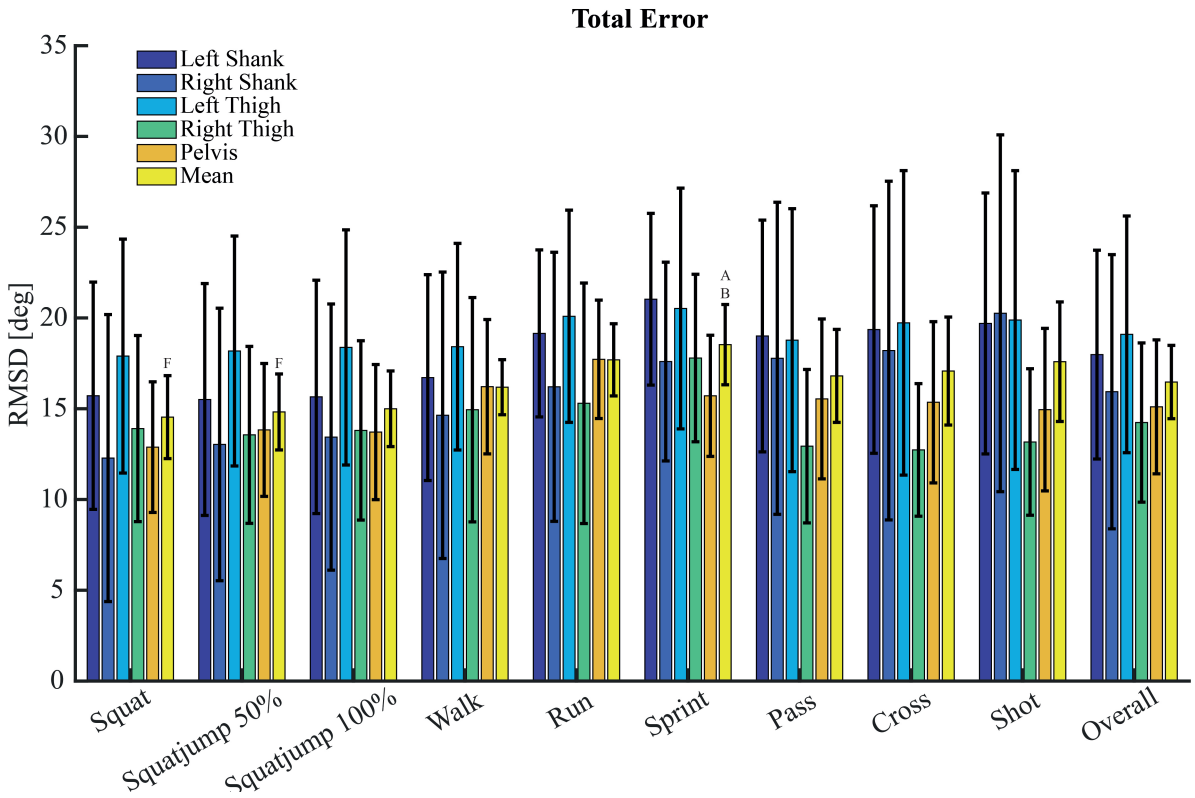

Fig. 11: Total error with sensor-body calibration A. Mean RMSD and STD for all body segments and all trials. Significant differences within each trial between body segments are displayed by letters above the bar, LS, RS, LT, RT and P mean a significant difference with the left shank, right shank, left thigh, right thigh and pelvis, respectively. Significant differences between trails are display with a letter above the mean bar. A = squat, B = squatjump 50%, C = squatjump 100%, D = walk, E = run, F = sprint, G = pass, H = cross and I = shot.

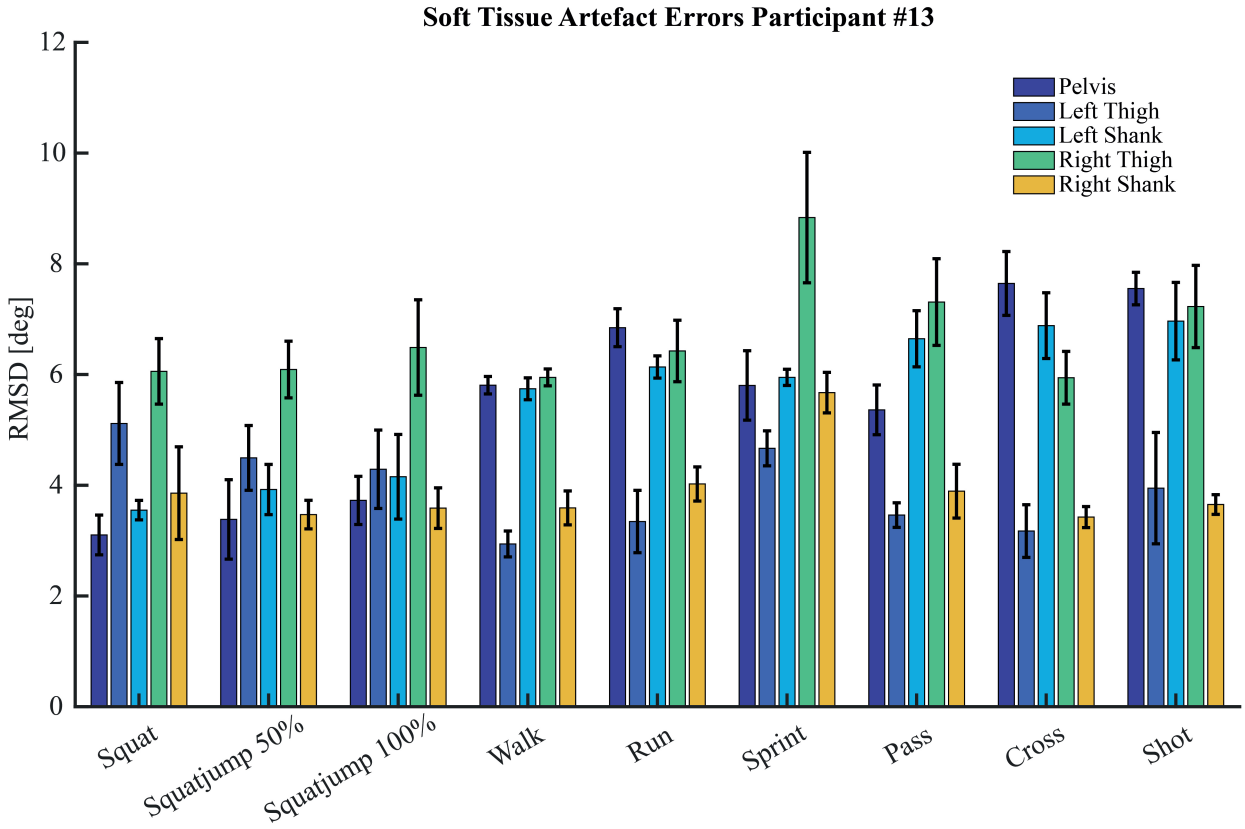

Fig. 12: Error caused by the STA of a typical subject. Mean RMSD and STD for all body segments and all trials.

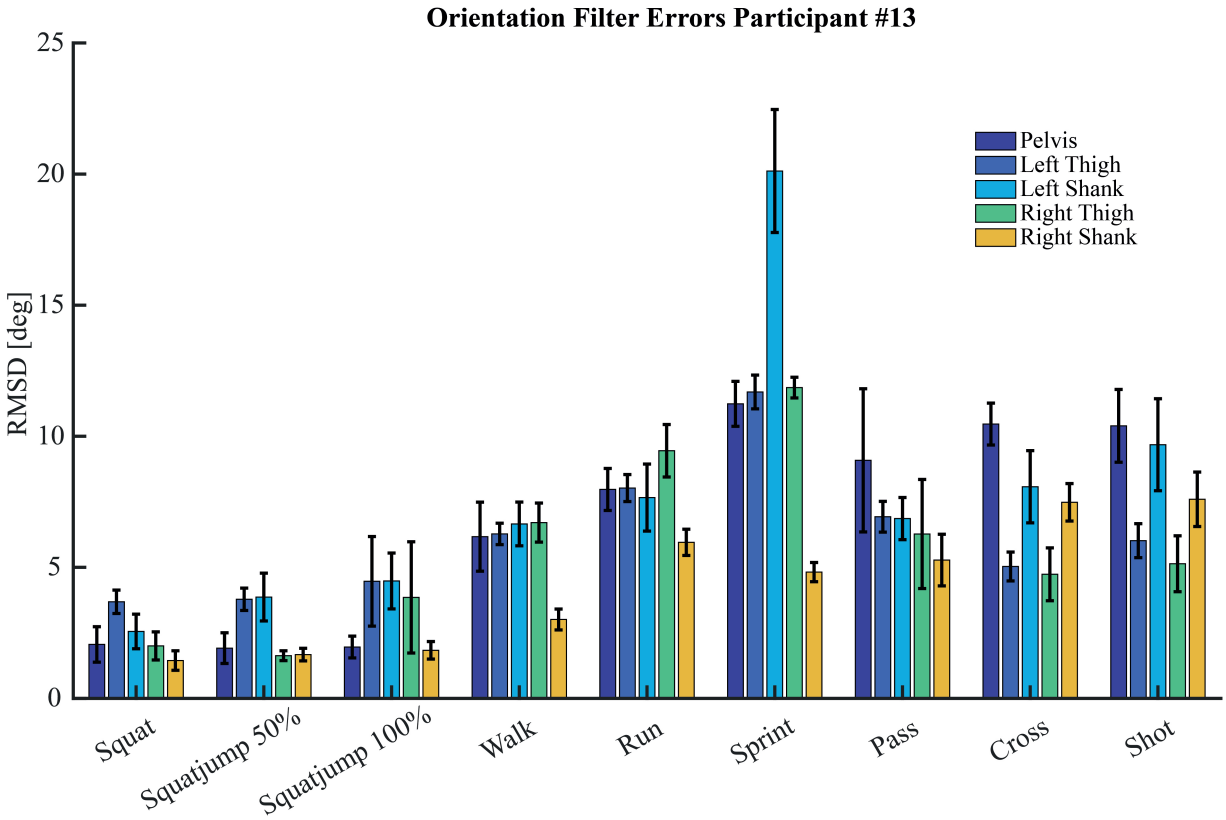

Fig. 13: Error caused by the orientation filter of a typical subject. Mean RMSD and STD for all body segments and all trials.